Material Matters™

Materials for Biomedical Applications

ALDRICH®
Materials Science

Making life better with materials that matter

Poly(*N*-isopropylacrylamide)-based Smart Surfaces for Cell Sheet Tissue Engineering

Patterning of PEG-based Hydrogels—Engineering Spatial Complexity

Conjugated Polymers for the Engineering of Device/Tissue Interface

The Progress in Development of Dental Restorative Materials

Strategy for Toxicity Screening of Nanomaterials

SIGMA-ALDRICH®

Introduction

Welcome to the third 2010 issue of *Material Matters™* entitled "Materials for Biomedical Applications," which highlights exciting scientific developments at the interface between the disciplines of materials science, medicine, chemistry, and biology. Professor David F. Williams (University of Liverpool) succinctly defines biomaterials as "nonviable materials used in medical devices, intended to interact with biological systems." In fact, biomaterials are rarely used as isolated materials but are more commonly integrated into devices or implants. The biological response to the final fabricated biomedical device will ultimately govern its success or failure. The field's rapid growth over the last half century was driven by advances in materials synthesis techniques combined with a rigorous application of engineering principles to the design of materials expressly for biomedical applications. Some of the developments and key enabling materials are presented in this issue.

Kaushik Patel, Ph.D.
Materials Science
Sigma-Aldrich Corporation

The issue begins with an article by Professors Françoise Winnik (University of Montreal) and Teruo Okano (Tokyo Women's Medical University) on the use of poly(*N*-isopropylacrylamide) as a thermally responsive grafting material for the harvesting of cell cultures used in tissue engineering. In the following article, Professor Mariah Hahn (Texas A&M University) describes the methods available to achieve 2D and 3D patterning of poly(ethylene glycol) hydrogels in order to control the placement of biochemical cues that guide the development of functional tissues. Professor David Martin and his colleagues from the University of Delaware discuss electrical interfacing of tissues with implantable electrostimulation devices using conjugated thiophene polymers. Moving toward new R&D opportunities for materials engineers, Professors James Stansbury and Christopher Bowman (University of Colorado) describe recent progress in the development of monomers and polymers for dental restorative composites. Currently, many of the composite materials are engineered at the nanoscale. To conclude the issue, a research team led by Professors Andre Nel and Jeffrey Zink from UCLA reports on their high-throughput strategy for the toxicity screening of nanomaterials, addressing a concern critical to the application of nanotechnology in medicine.

More than any other area of materials science, biomedical materials is an interdisciplinary field, and research is done by scientists of different backgrounds including materials and chemical engineers, biologists and chemists. Progress in this field critically depends on the transfer of knowledge and communication between disciplines, as well as the consistent, wide-spread availability of materials to facilitate the research. The team at Aldrich® Materials Science understands this problem, in part because our group includes scientists from diverse backgrounds including chemistry, materials science and biophysics. Thus, as we continue to invest and expand the Aldrich Materials Science product offer, we dedicate special attention to products for biomaterials research. For example, our Polymer Center of Excellence develops novel and exciting polymers designed specifically for use in biomedical applications (for example, NIPAM polymers presented in product tables on page 59.

Each article in this issue is accompanied by a list of materials available from Aldrich Materials Science. Please contact us at matsci@sial.com if you need materials that you cannot find in the catalog, or would like a custom grade for your development work.

About Our Cover

Some of the most promising areas in medical research, including regenerative/restorative medicine and drug delivery, are enabled by the development of key biomaterials. Ideal biomedical materials posses both the biological properties needed to interact with cellular environments, as well as the physical and chemical properties required for a desired application, e.g., strength and biological stability in the case of joint replacements. The creation of such materials begins with research at the molecular level. Two examples of materials tailored at the molecular level for medical uses are illustrated on the cover. The left box shows bone screws[1] made from biodegradable RESOMER® copolymers, composed of polylactide (shown in the right box) and polyglycolide. Additional stimuli-responsive polymeric materials are discussed in the NIPAM article on page 56.

(1) Center photo courtesy of Boehringer-Ingelheim

"Your Materials Matter."

**Joe Porwoll, President
Aldrich Chemical Co., Inc.**

Professor Nick Melosh of Stanford University kindly suggested that we offer *cis*-9-Octadecene-1-thiol (Aldrich Prod. No. 719692) as a product in our catalog. This molecule is designed to prepare disordered self-assembled monolayers that may have a significant influence on the fluidity of supported lipid membranes. A *cis*-double bond introduces a kink in the hydrophobic alkyl chains, disrupting the packing behavior compared to saturated alkyl thiol molecules and leading to disordered monolayers that mimic fluid biological lipid membranes.[1,2] Such monolayers can be used as supports for deposition of model lipid membranes on the monolayer-modified substrates.[3] The terminal thiol group of the *cis*-9-Octadecene-1-thiol allows for either assembly onto gold surfaces[4] or functionalization with a wide variety of biological entities, for example using the thiol-ene chemistry or reactions with reactive double bonds of maleimide[5] and acryloyl compounds.[6]

References

(1) Rawicz, W.; Olbrich, K. C.; McIntosh, T.; Needham, D.; Evans, E. *Biophys. J.* **2000**, *79*, 328.
(2) Silvius. J. R. Thermotropic Phase Transitions of Pure Lipids in Model Membranes and Their Modifications by Membrane Proteins; John Wiley & Sons, Inc.: New York. 1982.
(3) Jans, K.; Van Meerbergen, B.; Reekmans, G.; Bonroy, K.; Annaert, W.; Maes, G.; Engelborghs, Y.; Borghs, G.; Bartic, C. *Langmuir* **2009**, *25*, 4564.
(4) Bain, C. D.; Troughton, E. B.; Tao, Y.-T.; Evall, J.; Whitesides, G. M.; Nuzzo, R. G. *J. Am. Chem. Soc.* **1989**, *111*, 321.
(5) Kosif, I.; Park, E.-J.; Sanyal, R.; Sanyal, A. *Macromolecules* **2010**, *43*, 4140.
(6) Dondoni, A. *Angew. Chem. Int. Ed.* **2008,** *47*, 8995.

cis-9-Octadecene-1-thiol, 97%

$$CH_3(CH_2)_6CH_2 \diagup \diagdown CH_2(CH_2)_6CH_2SH$$
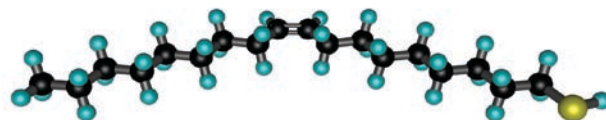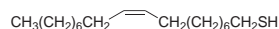
Oleyl mercaptan [31494-22-1]
$C_{18}H_{36}S$ FW 284.54
density...0.852 g/mL, 25 °C

719692-250MG	250 mg

Materials Featured in this Issue

Materials Category	Content	Page
Smart Polymers for Biomedical Applications	A selection of PolyNIPAM, poly(vinyl alcohols), and polymersome forming polymers	59
Biodegradable Polymers	A list of biodegradable polymers including RESOMER® materials by Boehringer-Ingelheim	60
Polyethylene Glycols	A selection of unfunctionalized, monofunctional, and bifunctional PEGs	64
Monomers for Conductive Polymers	Selected pyrrole and thiophene monomers used in the synthesis of conductive polymers	70
Conductive Polymers	A list of conductive polypyrroles and polythiophenes	72
Methacrylate Monomers	Selected methacrylate and methacrylamide monomers	77
Cross-Linkers	A selection of acrylic, thiol, and vinyl cross-linkers	78
Photoinitiators	A selection of organic photoinitiators	80
Amine Coinitiators	Selected tertiary amine coinitiators for Norrish Type II organic photoinitiators	81
Nanoparticles for Biomedical Applications	Selected nanomaterials including magnetic nanoparticles, quantum dots, metal oxides and ceramics as well as mesoporous materials and gold/silver nanomaterials	85

For questions, product data, or new product suggestions, please contact Aldrich Materials Science at *matsci@sial.com*.

ALDRICH®
Materials Science

55

Poly(N-isopropylacrylamide)-based Smart Surfaces for Cell Sheet Tissue Engineering

Masamichi Nakayama,[1] Teruo Okano,[1*] and Françoise M. Winnik[2**]

[1] Institute of Advanced Biomedical Engineering and Science, Tokyo Women's Medical University (TWIns), Kawada-cho 8-1, Shinjuku, Tokyo 162-8666, Japan
[2] Department of Chemistry and Faculty of Pharmacy, University of Montreal, CP 6128 Succursale Centre Ville, Montreal QC Canada H3C 3J7
Email: *tokano@abmes.twmu.ac.jp **francoise.winnik@umontreal.ca

Introduction

Tissue engineering has become a key therapeutic tool in the treatment of damaged or diseased organs and tissues, such as blood vessels and urinary bladders.[1] Nonetheless, major challenges still need to be overcome, in particular the construction of tissues with high cell densities and the prevention of post-transplantation inflammation. A promising tissue engineering approach relies on the use of cell culture surfaces grafted with poly(N-isopropylacrylamide) (PNIPAM, Aldrich Prod. No. 535311).[2] The basic idea is that cell adhesion/detachment on PNIPAM-modified substrates can be achieved by a simple temperature switch (Figure 1).
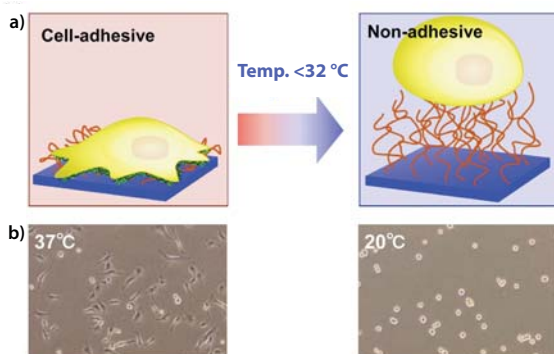
Figure 1. (a) Schematic representation of the adhesion (37 °C) and detachment (20 °C) of a cell on a poly(N-isopropylacrylamide)-grafted surface. Cell harvest is achieved simply by lowering the temperature. (b) Micrographs of endothelial cells on PNIPAM-coated dishes at 37 °C and 20 °C. Note the elongated shape of cells on the left micrograph characteristic of a supported cell culture, and rounded cell shape on the right characteristic of free cells in solution.

Cultured cells can be harvested from the "smart" PNIPAM surfaces in the form of a tissue-like cellular monolayer or "cell sheet" simply by lowering the cell culture temperature from 37 °C to 20 °C once confluency has been achieved. This cell manipulation technology enables the transplantation of cell sheets to host tissues without the use of biodegradable polymer scaffolds, overcoming a major constraint of conventional tissue engineering. The chemistry that underlies this process is described in this article, starting with a brief review of the properties of PNIPAM in aqueous solution. Special emphasis is placed on the design and fabrication of modified surfaces used to obtain multifunctional cell sheets.

Poly(N-isopropylacrylamide): The Ubiquitous "Smart" Polymer

PNIPAM is soluble in organic solvents, such as chloroform, acetone, methanol, and various other alcohols. It is also soluble in water, as long as the solution is kept reasonably cold. Heating an aqueous PNIPAM solution past 32 °C (the cloud point (CP) or lower critical solution temperature (LCST)) instantaneously converts the clear solution into a milky suspension. The phenomenon is reversible: as soon as the milky suspension is cooled below 32 °C it recovers its clarity.[3] In the late 1960s, Heskins and Guillet published the first phase diagram of the water/PNIPAM system, which they constructed by measuring the phase transition temperature as a function of PNIPAM concentration.[4] At about the same time, it became known that crosslinked PNIPAM networks (gels) also exhibit curious properties in water: they are highly swollen in cold water, but shrink as soon as they are heated above 32 °C. As in the case of PNIPAM solutions, the behavior of the gels is reversible, swelling back to their original volume, as soon as they are cooled below 32 °C. Hundreds of swelling/shrinking cycles can be performed by a gel, with no sign of material fatigue. This unusual phenomenon was noticed by Allan S. Hoffmann, who was among the first to use the temperature-induced phase transition of PNIPAM derivatives as a trigger to control phenomena relevant to biomedical applications, such as the release of a dye or drug.[5] This pioneering work laid the foundation of the field of responsive systems, which continues to captivate the imagination of scientists.[6] The heat-induced phase transition exhibited by aqueous PNIPAM solutions is not unique, as many other water-soluble polymers have cloud points. However, PNIPAM remains the leader for biomedical applications because of the sharpness of the transition, a transition temperature that is close to body temperature, the robustness of the polymer itself, and the availability of information on the polymer and its phase transition.
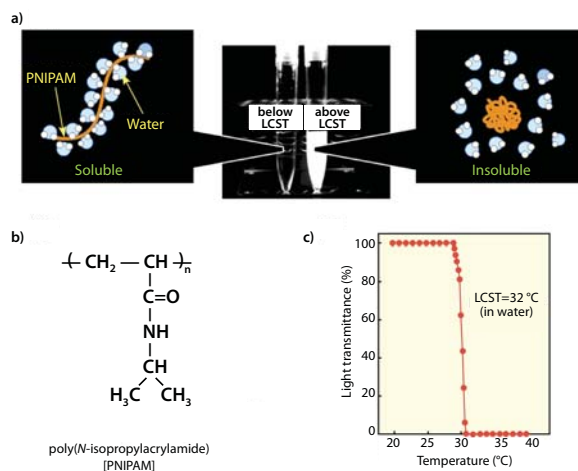
Figure 2. Temperature-responsive properties of aqueous poly(N-isopropylacrylamide) (PNIPAM) solutions; (a) when heated above the LCST, the hydrated extended PNIPAM chain collapses into a hydrophobic globule with simultaneous release of the bound water molecules; (b) chemical structure of the repeat unit of PNIPAM; (c) Plot of the changes in solution transmittance as a function of temperature for a PNIPAM solution in water. The LCST corresponds to the mid-point of the transition curve.

On the molecular level, the macroscopic phase transition corresponds to the dehydration of the PNIPAM chains and subsequent collapse of the denuded hydrophobic chains into compact globules that aggregate into larger mesoglobules (Figure 2).[7,8] However, the phase transition is not solely dependent upon the temperature-induced molecular rearrangement. Several other factors can affect the CP of PNIPAM, although the effects are not always predictable.

Molecular Weight—The extent of the affect of polymer molecular weight on the cloud point has been debated. There are some reports indicating that the cloud point of PNIPAM in water is directly related to molecular weight, while others report an inverse dependence of the CP on molecular weight and still others report that the CP of aqueous PNIPAM solutions are independent of molecular weight. The differences are particularly striking when comparing the results obtained for relatively short polymer chains (M_w <20,000 g/L) for which the chemical nature of the chain end has a significant impact on the CP value.[9] Polymers with hydrophilic end groups tend to exhibit a relatively high cloud point in the low concentration solutions, whereas polymers with hydrophobic end groups usually have lower CPs under the same conditions.[10] These trends break down for solutions of PNIPAMs with strongly hydrophobic end groups, such as n-octadecyl chains, which self-assemble in water to form flower and star micelles.[11,12]

Solvent Systems—The presence of multi-solvent systems can also have an impact on the CP of PNIPAMs. For example, at room temperature, PNIPAM is not soluble in a water/methanol mixed solution over a range of compositions—exhibiting a phenomenon called co-nonsolvency.[13]

Presence of Salts—The presence of salts can also affect the CP of aqueous PNIPAM solutions, with some salts causing an increase in the CP, while the addition of other salts yield a CP decrease. Several explanations have been offered to account these observations.[14] Once the factors affecting the phase transition of the PNIPAM are fully understood, then they can be used to tailor and optimize PNIPAMs for further applications. However, exciting uses of this smart polymer have already been uncovered.

Temperature-responsive Cell Culture Dish for Cell Sheet Engineering

PNIPAM-coated cell culture dishes are prepared by electron beam irradiation (0.3 MGy at 150 kV) of NIPAM monomer (Aldrich Prod. No. 724459), deposited on commercial tissue culture polystyrene (TCPS) cell culture dishes from a NIPAM solution in 2-propanol (Figure 3). This treatment results in simultaneous polymerization of NIPAM and covalent grafting of the growing polymer chains on the TCPS surfaces. The method is clean, readily amenable to scale-up and patterning, and it allows fine control over the polymer layer thickness. For most cell culture applications, the thickness of grafted PNIPAM layer should be within the 15–20 nm range, which corresponds to a grafting density of 1.4–2.0 μg/cm^2.[15]

Electron beam (0.3 MGy)

PNIPAM-grafted layer

polymerization and grafting

A solution of NIPAM in 2-propanol (55 wt%) is spread on TCPS dish

The PNIPAM-grafted dish is washed with cold water and sterilized with ethylene oxide gas
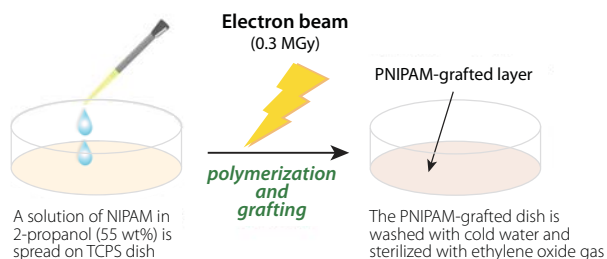
Figure 3. Schematic of the preparation procedure for poly(*N*-isopropylacrylamide)-grafted cell culture dishes.

Various cell types adhere and grow on temperature-responsive PNIPAM culture surfaces under culture conditions similar to those used with ordinary TCPS dishes. After reaching cell confluency at 37 °C, the dishes are cooled below 32 °C (typically to 20 °C). The polymer chains rehydrate and repel the cells, inducing the cells to peel off from the culture surface in the form of a cell sheet comprised of a contiguous monolayer of cells. In conventional cell-based tissue engineering, proteolytic enzymes (e.g., trypsin and dispase) are added to the culture medium in order to detach the cells by disruption of cell adhesion molecules and extracellular matrix (ECM) proteins. This treatment can also affect the cell membrane proteins that are vital to the distinctive functions of various cell types. No enzymatic treatment is necessary to harvest cells cultured on temperature-responsive surfaces. Hence, the recovered cell sheets, which still possess their basal ECM proteins, can be transferred onto new culture dishes, other cell sheets, or living tissues. Several cell sheet tissue engineering clinical trials are in progress using transplantation of single cell sheets, such as cornea and periodontal ligament. Ongoing studies include homo- and heterotypic layering of multiple cell sheets to create 3D tissue-like architectures, such as heart or liver tissues.[16]

Patterned Temperature-responsive Surfaces for Heterotypic Cell Co-Culture

To mimic specific tissue functions, it is necessary to regenerate spatially ordered tissue architectures with heterotypic cell-cell interactions. It is not easy to integrate multiple cell types within a single 3D tissue architecture, since the adhesion and proliferation properties of different cell types are usually not the same. In most cases, co-culture of different cell types is carried out on micropatterned surfaces. Temperature-responsive micropatterned surfaces are easily fabricated based on the fact that the LCST of PNIPAM can also be modulated by incorporation of a comonomer. NIPAM copolymers with hydrophilic comonomers have an LCST >32 °C, while NIPAM copolymers incorporating a hydrophobic monomer, such as *n*-butyl methacrylate (BMA), have an LCST <32 °C. To prepare a micropatterned surface, a solution of BMA (Aldrich Prod. No. 235865) in 2-propanol is spread over a PNIPAM-grafted TCPS dish. Subsequently, the BMA-coated surface is irradiated with an electron beam through a stainless steel micropatterned mask.[17] The BMA monomers are grafted onto the preformed PNIPAM layer in the irradiated areas, in contrast to the masked sections, where the original PNIPAM is preserved. The transition temperature of the irradiated areas is lower than 32 °C. The actual LCST value is modulated by controlling the level of BMA incorporation. An application of this patterning method for the co-culture of hepatocytes (HC) and endothelial cells (EC) is depicted in Figure 4.
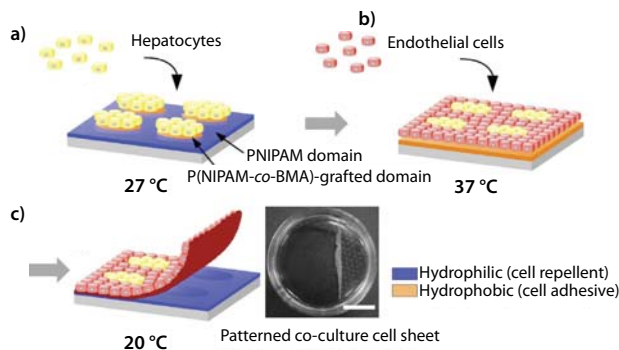
Figure 4. Schematic representation of pattern-wise cell co-culture and harvest of a co-cultured cell sheet using a patterned temperature-responsive surface. (a) Hepatocytes (HCs) are seeded and cultured at 27 °C, resulting in localization of HCs onto P(NIPAM-*co*-BMA)-grafted islands showing hydrophobic nature. (b) Endothelial cells (ECs) are seeded and cultured at 37 °C generating patterned co-cultures. (c) Decreasing the temperature to 20 °C induces the detachment of the co-cultured cell sheet. Harvested patterned co-cultured cell sheet (right; scale bar: 1 cm).

For questions, product data, or new product suggestions, please contact Aldrich Materials Science at *matsci@sial.com*.

ALDRICH® Materials Science

57

First, HCs are seeded on a micropatterned interface kept at 27 °C. They adhere exclusively onto the P(NIPAM-co-BMA) domains, which are dehydrated (hydrophobic) at this temperature. The PNIPAM domains, which are hydrated (hydrophilic) at 27 °C, repel the cells (Figure 4a). Next, the HC-coated interface is heated to 37 °C. The PNIPAM domains become hydrophobic and ECs are seeded. They adhere to the PNIPAM domains and proliferate, (Figure 4b and 4c). Lowering the culture temperature to 20 °C triggers the hydration of the entire surface. The co-cultured cell monolayer detaches spontaneously, yielding a continuous cell sheet with heterotypic cellular interactions. The recovered co-cultured cell sheets can be manipulated and sandwiched between other cell sheets for the preparation of tissue-mimicking multi-layered materials.

Functionalization of a Temperature-responsive Culture Dish

Chemically-reactive (functional) comonomers can be incorporated into the grafted PNIPAM layer and serve as sites for the introduction of bioactive molecules, as exemplified in Figure 5.[15]
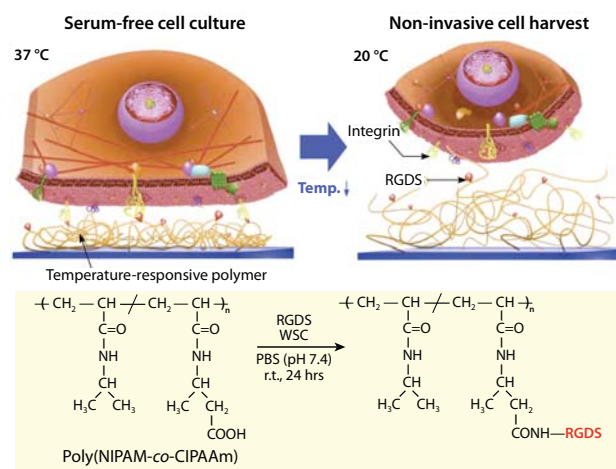
Figure 5. Schematic illustration of the temperature-responsive affinity control between integrin receptors and RGDS (Arg-Gly-Asp-Ser) peptides. RGDS ligands are conjugated to P(NIPAM-co-CIPAAm) using amide bond formation with N-(3-dimethylaminopropyl)-N'-ethylcarbodiimide hydrochloride (water-soluble carbodiimide (WSC, Aldrich Prod. No. E1769) as a coupling reagent. At 37 °C, the temperature-responsive polymer shrinks to expose RGDS ligands (red beads) to the cell membrane integrin receptors (yellow). Thus, cells can be cultured in serum-free conditions on RGDS-immobilized temperature-responsive culture dishes. By decreasing the culture temperature to 20 °C, cells are harvested non-invasively. The RGDS ligands remain attached to the temperature-responsive polymer surface.

First, TCPS dishes are grafted with a copolymer of NIPAM and 2-carboxyisopropylacrylamide (CIPAAm) by electron beam polymerization of a NIPAM/CIPAAm mixture (CIPAAm content: 1–5 mol%). Subsequently, the synthetic cell adhesion tetrapeptide, Arg-Gly-Asp-Ser (RGDS, Sigma Prod. No. A9041) is linked covalently to the P(NIPAM-co-CIPAAm) grafted TCPS dish, using standard amide bond formation methodologies.[18] The presence of RGDS on the interface promotes cell

adhesion and growth to confluency at 37 °C under the serum-free culture conditions supplemented with recombinant growth factors. After reaching confluency, cells can be harvested as intact cell sheets by simply reducing the temperature to 20 °C, as in the case of PNIPAM-grafted culture dishes. Rehydration of the PNIPAM surface chains irreversibly disrupts the interactions between the surface-immobilized RGDS peptides and the cell membrane integrin receptors. This strategy significantly reduces the culture period and allows for the growth of cells in the absence of the traditional fetal bovine serum, which is an important consideration given the potential risks associated with the use of mammalian-sourced products in the manufacture of tissues used in clinical applications for human cell therapies.

Conclusions

Future progress in temperature-responsive cell sheet engineering depends on the availability of precisely optimized PNIPAM-grafted surfaces enabling the controlled fabrication of heterotypic cell sheets. One promising approach relies on the use of PNIPAM brushes of controlled thickness and grafting density prepared by controlled radical polymerization, such as atom transfer radical polymerization (ATRP) and reversible addition-fragmentation chain transfer (RAFT) polymerization.[19-21] The development of these novel smart surfaces and their research and medical use will open up new frontiers in the biological and medical fields.

References
(1) Vacanti, C. A. MRS Bulletin 2001, 26, 798.
(2) Yamada, N.; Okano, T.; Sakai, H.; Karikusa, F.; Sawasaki, Y.; Sakurai, Y.; Makromol. Chem. Rapid Commun. 1990, 11, 571.
(3) Schild, H. G. Prog. Polym. Sci. 1992, 17, 163.
(4) Heskins, M.; Guillet, J. E. Macromol. Sci. Chem. A 1968, 2, 1441.
(5) Ding, Z.; Chen, G.; Hoffman, A. Bioconjugate Chem. 1996, 7, 121.
(6) Cohen Stuart, M. A.; Huck, W. T. S.; Genzer, J.; Müller, M.; Ober, C.; Stamm, M.; Sukhorukov, G. B.; Szleifer, I.; Tsukruk, V. V.; Urban, M.; Winnik, F. M.; Zauscher, S.; Luzinov, I.; Minko, S. Nat. Mater. 2010, 9, 101.
(7) Okada, Y.; Tanaka, F. Macromolecules 2005, 38, 4465.
(8) Kujawa, P.; Aseyev, V.; Tenhu, H.; Winnik, F. M. Macromolecules 2006, 39, 7686.
(9) Xia, Y.; Burke, N. A. D.; Stover, H. D. H. Macromolecules 2006, 39, 2275.
(10) Duan, Q.; Miura, Y.; Narumi, A.; Shen, X.; Sato, S.-I.; Satoh, T.; Kakuchi, T. J. Polym. Sci., Part A: Polym. Chem. 2006, 44, 1117.
(11) Kujawa, P.; Segui, F.; Shaban, S.; Diab, C.; Okada, Y.; Tanaka, F.; Winnik, F. M. Macromolecules 2006, 39, 341.
(12) Kujawa, P.; Tanaka, F.; Winnik, F. M. Macromolecules 2006, 39, 3048.
(13) Tanaka, F.; Koga, T. ; Kojima, H. ; Winnik, F. M. Macromolecules 2009, 42, 1321.
(14) Zhang, Y.; Furyk, S.; Bergbreiter, D. E.; Cremer, P. S. J. Am. Chem. Soc. 2005, 127, 14505.
(15) Akiyama, Y.; Kikuchi, A.; Yamato, M.; Okano, T. Langmuir 2004, 20, 5506.
(16) Yang, J.; Yamato, M.; Nishida, K.; Ohki, T.; Kanzaki, M.; Sekine, H.; Shimizu, T.; Okano, T. J. Controlled Release 2006, 116, 193.
(17) Tsuda, Y.; Kikuchi, A.; Yamato, M.; Chen, G.; Okano, T. Biochem. Biophys. Res. Commun. 2006, 348, 937.
(18) Ebara, M.; Yamato, M.; Aoyagi, T.; Kikuchi, A.; Sakai, K.; Okano, T. Biomacromolecules 2004, 5, 505.
(19) Mizutani, A.; Kikuchi, A.; Yamato, M.; Kanazawa, H.; Okano, T. Biomaterials, 2008, 29, 2073.
(20) Takahashi, H.; Nakayama, M.; Yamato, M.; Okano, T. Biomacromolecules, ASAP
(21) For a brief introduction to ATRP and RAFT polymerizations, please see Material Matters™ 2010, Vol. 5, No. 1.

Smart Polymers for Biomedical Applications

For a complete list of available polymers, please visit *aldrich.com/poly*

Poly(*N*-isopropylacrylamide) (PNIPAM) Materials

Name	Structure	Molecular Weight	Cat. No.
Poly(*N*-isopropylacrylamide)		M_n 10,000-15,000	724459-5G
Poly(*N*-isopropylacrylamide)		M_n 20,000-25,000	535311-10G
Poly(*N*-isopropylacrylamide), amine terminated		average M_n 2,500	724823-1G 724823-5G
Poly(*N*-isopropylacrylamide), amine terminated		average M_n 5,500	724831-1G 724831-5G
Poly(*N*-isopropylacrylamide), carboxylic acid terminated		average M_n 2,000	724815-1G 724815-5G
Poly(*N*-isopropylacrylamide), carboxylic acid terminated		average M_n 5,000	724807-1G 724807-5G
Poly(*N*-isopropylacrylamide), carboxylic acid terminated		average M_n 7,000	724866-1G 724866-5G
Poly(*N*-isopropylacrylamide), maleimide terminated		average M_n 2,000	731048-1G 731048-5G
Poly(*N*-isopropylacrylamide), maleimide terminated		average M_n 4,000	728632-1G 728632-5G
Poly(*N*-isopropylacrylamide), *N*-hydroxysuccinimide (NHS) ester terminated		average M_n 2,000	725668-1G 725668-5G
Poly(*N*-isopropylacrylamide-*co*-methacrylic acid)		M_n 40,000-60,000	724467-5G
Poly(*N*-isopropylacrylamide-*co*-methacrylic acid)		M_n 40,000-80,000	724858-5G
Poly(*N*-isopropylacrylamide-*co*-methacrylic acid-*co*-octadecyl acrylate)		M_n 30,000-60,000	724475-5G
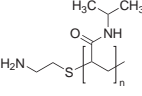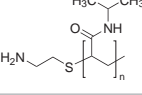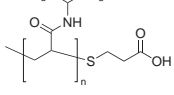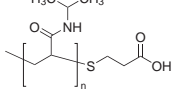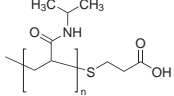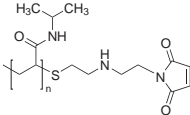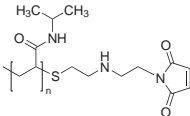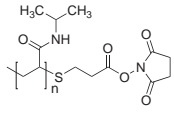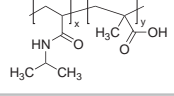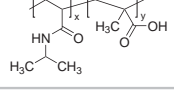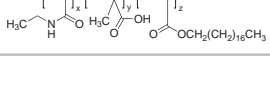
For questions, product data, or new product suggestions, please contact Aldrich Materials Science at *matsci@sial.com*.

59

Poly(vinyl alcohols)

Name	Structure	Molecular Weight	% Hydrolyzed	Cat. No.
Poly(vinyl alcohol)		M_w 9,000-10,000	80%	360627-25G 360627-500G 360627-1KG
Poly(vinyl alcohol)		M_w 13,000-23,000	87-89%	363170-25G 363170-500G 363170-1KG
Poly(vinyl alcohol)		M_w 31,000-50,000	98-99%	363138-25G 363138-500G 363138-1KG
Poly(vinyl alcohol)		M_w 89,000-98,000	99+%	341584-25G 341584-500G 341584-1KG
Poly(vinyl alcohol)		M_w 85,000-124,000	99+%	363146-25G 363146-500G 363146-1KG
Poly(vinyl alcohol)		average M_w 130,000	99+%	563900-500G 563900-1KG
Poly(vinyl alcohol)		M_w 146,000-186,000	99+%	363065-25G 363065-500G 363065-1KG

Polymersome Forming Polymers

Name	Structure	Molecular Weight	Cat. No.
Poly(styrene)-block-poly(acrylic acid)		M_n 5,580-6,820 (polystyrene) M_n 1,890-2,310 (poly(acrylic acid)) M_n 7,470-9,130	686794-500MG
Poly(styrene)-block-poly(ethylene glycol)		M_n 20,700-25,300 (polystyrene) M_n 800-1,200 (PEG) M_n 22,500-27,500	686476-500MG

Biodegradable Polymers

Name	Structure	Molecular Weight	Cat. No.
Poly(L-lactide), ester terminated inherent viscosity 0.8-1.2 dL/g* (RESOMER® L 206 S)		-	719854-5G 719854-25G
Poly(L-lactide), inherent viscosity ~0.5 dl/g		M_n 50,400 M_w 67,400	94829-1G-F 94829-5G-F
Poly(L-lactide), inherent viscosity ~1.0 dl/g		M_n 59,100 M_w 101,700	93578-1G-F 93578-5G-F
Poly(L-lactide), inherent viscosity ~2.0 dl/g		M_n 99,000 M_w 152,000	81273-10G
Poly(L-lactide), inherent viscosity ~4.0 dl/g		M_n 103,200 M_w 258,700	95468-1G-F 95468-5G-F 95468-25G-F
Poly(DL-lactide), ester terminated* (RESOMER® R 202 S)		M_w 10,000-18,000	719951-1G 719951-5G

Name	Structure	Molecular Weight	Cat. No.
Poly(D,L-lactide), ester terminated* (RESOMER® R 203 S)		M_w 18,000-28,000	719935-1G 719935-5G
Poly(D,L-lactide), acid terminated* (RESOMER® R 203 H)		M_w 18,000-24,000	719943-1G 719943-5G
Poly(D,L-lactide), acid terminated* (RESOMER® R 202 H)		M_w 10,000-18,000	719978-1G 719978-5G
Poly(dioxanone), viscosity 1.5-2.2 dL/g* (RESOMER® X)		-	719846-1G 719846-5G
Polyglycolide, inherent viscosity 1.4-1.8 dL/g		-	457620-5G
Poly(DL-lactide-co-glycolide), 85:15 lactide:glycolide		M_w 50,000-75,000	430471-1G 430471-5G
Poly(DL-lactide-co-glycolide), acid terminated, (75:25)* (RESOMER® RG 752 H)		M_w 4,000-15,000	719919-1G 719919-5G
Poly(DL-lactide-co-glycolide), ester terminated, (75:25)* (RESOMER® RG 756 S)		M_w 76,000-115,000	719927-1G 719927-5G
Poly(DL-lactide-co-glycolide), acid terminated, (65:35)* (RESOMER® RG 653 H)		M_w 24,000-38,000	719862-1G 719862-5G
Poly(DL-lactide-co-glycolide), acid terminated, (50:50)* (RESOMER® RG 502 H)		M_w 7,000-17,000	719897-1G 719897-5G
Poly(DL-lactide-co-glycolide), ester terminated, (50:50)* (RESOMER® RG 502)		M_w 7,000-17,000	719889-1G 719889-5G
Poly(DL-lactide-co-glycolide), acid terminated, (50:50)* (RESOMER® RG 503 H)		M_w 24,000-38,000	719870-1G 719870-5G
Poly(DL-lactide-co-glycolide), acid terminated, (50:50)* (RESOMER® RG 504 H)		M_w 38,000-54,000	719900-1G 719900-5G
Polylactide-block-poly(ethylene glycol)-block-polylactide		PEG average M_n 900 PLA average M_n 3,000 (total)	659630-1G
Polylactide-block-poly(ethylene glycol)-block-polylactide		PEG average M_n 10,000 PLA average M_n 2,000	659649-1G

*RESOMER® Products of Boehringer-Ingelheim

For questions, product data, or new product suggestions, please contact Aldrich Materials Science at *matsci@sial.com*.

ALDRICH® Materials Science

61

Patterning of PEG-based Hydrogels—Engineering Spatial Complexity

Mariah S. Hahn
Department of Chemical Engineering, Texas A&M University
200 Jack E. Brown Bldg, 3122 TAMU
College Station, TX 77843-3122
Email: mhahn@tamu.edu

Introduction

Most biomaterial scaffolds developed for tissue engineering applications are relatively homogeneous and lack the complexity and organization of the *in vivo* cellular microenvironment. While these homogeneous scaffolds have enabled remarkable progress in understanding cell responses to their microenvironment, elucidating the dynamic relationship between biomaterial properties and their influence on biological function may require more spatially and temporally complex scaffolds. Thus, various patterning methods have been developed to permit control over the presentation of biochemical and biomechanical cues in both space and time. To explore the cell responses to dynamic alterations in 3D matrix properties, scaffold modifications must be performed in a manner compatible with the maintenance of cell viability. Therefore, many of the patterning techniques applied to silicon and glass substrates cannot be readily transitioned to these applications. In this article, we will discuss the benefits and limitations of several 2D and 3D scaffold patterning techniques that can be applied in the presence of cells. Although these methods will be discussed in the context of poly(ethylene glycol) (PEG)-based hydrogels, they can technically be applied to any optically transparent, photoactive substrate.

Hydrogels are a class of biomaterial scaffolds that have been widely used in complex device fabrication, drug release, and tissue engineering. PEG-based hydrogels, in particular, have proven extremely versatile for tissue engineering applications. PEG is FDA approved for a variety of applications and exhibits high biocompatibility and little or no immunogenicity. In addition, PEG-based hydrogels display tunable mechanical properties in the range appropriate to soft tissue regeneration. Importantly for patterning applications, PEG-based hydrogels are intrinsically resistant to protein adsorption and cell adhesion, thus providing biological "blank slates" upon which desired biofunctionality can be built.[1] To generate PEG hydrogels, individual PEG chains that have been functionalized with two or more crosslinkable groups, such as acrylates, are dissolved in aqueous solution, mixed with appropriate photoinitiator (e.g., 2,2 dimethoxy-2-phenyl acetophenone), and exposed to UV or visible light.[2,3] The acrylate groups cross-link via free radical polymerization to form an insoluble hydrogel network. These polymerization processes require between 1 and 10 minutes of illumination, depending on the photoinitiator and the intensity of the light source, and can be conducted under mild conditions that allow maintenance of cell viability. Although the polymerization process is rapid, its efficient quenching by oxygen and other free radicals is believed to maintain the spatial localization of the light-induced polymerization, which is essential to high fidelity pattern formation.

Patterning of the PEG-based hydrogels can be broadly divided into two approaches, one focusing on fabricating hydrogel networks of complex geometries and another focused on spatially and temporally modifying existing (pre-formed), cell-laden hydrogel structures.[4-16] Development of the latter approach, which will be the focus of this review, is particularly critical to understanding the spatial and temporal role of biomechanical versus biochemical signals in cell function as well as in complex tissue regeneration. In the following discussion, the term "2D patterning" will refer to the formation of patterns that vary in x-y directions but are uniform in the z direction, whereas the term "3D patterning" will refer to the generation of patterns that can vary in x, y, and z. In other words, these terminologies refer to the dimensionality of the spatial variations of the pattern rather than to the dimensionality of the patterned substrates.

Two-dimensional Patterning Methods

Transparency-based photolithography is one approach for creating 2D biochemical and biomechanical patterns within existing hydrogel structures. In one embodiment of this strategy, a hydrogel is prepared from PEG-diacrylate (PEGDA, Aldrich Prod. Nos. 701971, 701963) in such a manner as to leave sufficient free acrylate groups available for subsequent reactions.[10] The acrylated moieties to be patterned are then applied to the surfaces of these "incompletely" polymerized gels and a transparency photomask is placed in direct contact with the hydrogel surface. Following hydrogel illumination through the photomask, mono-acrylated materials are covalently immobilized to the surface of the hydrogel in areas corresponding to light-permissive regions of the mask. Patterning of monoacrylated, cell-adhesive factors permits definition of specific regions for cell-material interactions while the unpatterned regions remain bioinert (Figure 1). Multiple cell adhesive peptides can be readily patterned onto the hydrogel surface by sequential application of this method.[10,15]
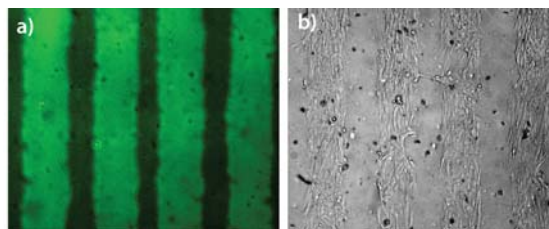
Figure 1. Transparency-based patterning. (a) Pattern of fluorescently labeled, monoacrylate-derivatized cell adhesion peptide Arg-Gly-Asp-Ser (RGDS) formed on the surface of an existing PEGDA hydrogel network using transparency-based photo-lithography. (b) Associated human dermal fibroblast surface adhesion demonstrating that unpatterned regions remain bioinert.

As demonstrated by West and coworkers, if the acrylated species are allowed to diffuse into the hydrogel network prior to illumination, the resulting pattern will extend through the full thickness of the gel and can be used to control cell behavior internal to the hydrogel (Figure 2).[11] Furthermore, if the entities to be patterned are functionalized with two or more acrylate groups, regional alterations in hydrogel biomechanical properties can be achieved.[11]
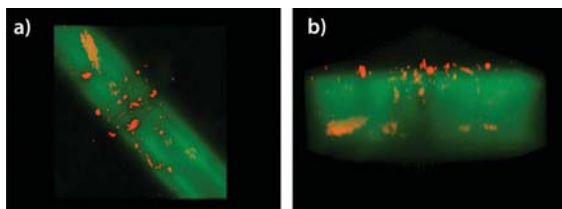
Figure 2. Cell migration confined to channels patterned using transparency-based photolithography with monoacrylate-derivatized, fluorescently-labeled RGDS. These patterned channels were created within a pre-formed collagenase-degradable PEGDA hydrogel. (a) A top view of a 3D OsiriX volume rendering of a confocal image series (z-stack) of the patterned hydrogels (acrylate-derivatized RGDS (green) and HT-1080 cell clusters (red-orange)). (b) A side view of a 3D OsiriX volume rendering of a confocal image series (z-stack) of the patterned hydrogels (acrylate-derivatized RGDS (green) and HT-1080 cell clusters (red-orange)). The apparent unevenness in RGDS intensity observed in (b) is primarily due, not to actual unevenness in RGDS patterning intensity, but to imaging artifacts.

In contrast to methods based on physical photomasks, the laser scanning capability of standard confocal microscopes can be used to generate 2D hydrogel surface patterns.[9] As in the method for transparency-based hydrogel patterning, acrylated species are applied to the surface of pre-formed, but incompletely polymerized PEGDA hydrogels. Computer control of the scanning lasers and of the laser shutter results in a so-called "virtual mask" in which laser light is applied only to desired regions of the hydrogel surface. As established by West and coworkers, the levels of acrylated species conjugated to the hydrogel surface can be spatially controlled by user adjustment of laser intensity or scanning speed, allowing for complex 2D concentration gradients to be formed (**Figure 3a**).[9] This level of spatial control over irradiation exposure is not readily achieved using conventional photolithographic masks. By incorporating intermediate wash steps between sequential irradiation cycles, multiple bioactive peptides can be patterned onto the hydrogel surface.[9] In addition, uniform cross-section patterns extending through scaffolds of moderate thickness can be created using a confined laser beam rather than a focused laser beam.[5]
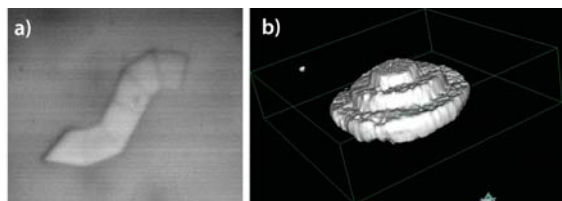
Figure 3. Standard laser scanning lithography and two-photon laser scanning lithography. (a) A gradient pattern of fluorescently labeled, monoacrylate-derivatized cell adhesion peptide RGDS formed of the surface of an existing PEGDA hydrogel network using the "virtual mask" capability of standard confocal microscopes. (b) A side view of a 3D OsiriX volume rendering of a confocal image series (z-stack) of a hydrogel patterned with fluorescently labeled, acrylate-derivatized RGDS (white) using a confocal microscope equipped with a two photon laser.

Three-dimensional Patterning Methods

The above-described methods are limited to the creation of vertically uniform patterns. To program the spatial complexity mimetic of native tissue into pre-formed hydrogels, researchers have turned to two photon-based patterning. The phenomenon of two-photon absorption has enabled the development of 3D fluorescence imaging and 3D lithographic microfabrication. Both of these applications take advantage of the fact that, by tightly focusing an excitation beam, the region of two photon adsorption can be confined to a focal volume roughly half the excitation wavelength in dimension. Any subsequent process, such as a photoinitiated, radical-based polymerization, is also localized to this small volume, assuming the time-scale of radical diffusion is large compared to the radical half-life. Thus, by specifying the location of the focal point of a two-photon laser beam, regions of photo-induced conjugation can be precisely dictated. This is in contrast to "standard" lasers in which photo-induced conjugation can occur outside the focal

plane. Multiphoton laser modules are now available for most commercial confocal microscopes, allowing the laser scanning and shuttering capacity associated with these instruments to be readily applied to two-photon based patterning.

To create 3D patterns within existing hydrogel networks, incompletely polymerized PEGDA hydrogels are once again prepared and acrylated moieties are allowed to diffuse into the gel network, after which the hydrogel is placed on the confocal microscope stage and two-photon laser scanning is initiated. By varying the irradiation exposure time or beam intensity during the two photon patterning cycle, the levels of modification can be spatially tailored.[11,16] Following polymerization, residual precursors are allowed to diffuse out of the hydrogel to reveal a heterogeneously-distributed patterned molecule (**Figure 3b**).[11]

Extended Chemistries

The above-described methods for 2D and 3D PEGDA hydrogel patterning rely on the same chemistry to both generate the PEG hydrogel and to conjugate various species to the gel networks. However, in this strategy, the patterning process itself further alters the initial gel structure, and the extent of network modification is limited by the availability of unreacted acrylate groups. Furthermore, although desired bioactive moieties can be added on demand, these chemistries do not enable ready removal of bioactive signals. To address these limitations, Anseth and co-workers have developed alternative chemistries that permit the synthesis of well-defined cross-linked hydrogels in which the physical and chemical properties of hydrogel are independently controlled.[12-14] Essentially these strategies involve exploiting "orthogonal chemistries," where one chemistry is used to generate the hydrogel network and a second chemistry is used to pattern in bioactive factors. Furthermore, the introduction of photolabile links within the hydrogel networks has enabled the removal of added bioactive signals at desired time points.[14]

Combined, the above-described 2D and 3D patterning methods enable the controlled investigation of the dynamic relationship between biomaterial properties and their influence on biological function. Advances in our understanding of cell behavior which result from studies using these patterned scaffold systems will enable intelligent design of scaffold properties for regenerative medicine applications.

Acknowledgments

References
(1) Gombotz, W. R.; Wang, G. H.; Horbett, T. A.; Hoffman, A. S. *J. Biomed. Mater. Res.* **1991,** *25,* 1547-62.
(2) West, J. L.; Hubbell, J. A. *Biomaterials* **1995,** *16,* 1153-1156.
(3) Hill-West, J. L.; Chowdhury, S. M.; Slepian, M. J.; Hubbell, J. A. *Proc. Natl. Acad. Sci. USA* **1994,** *91,* 5967-71.
(4) Lu, Y.; Mapili, G.; Suhali, G.; Chen, S.; Roy, K. *J. Biomed. Mater. Res., Part A* **2006,** *77A,* 396-405.
(5) Luo, Y.; Shoichet, M. *Nat. Mater.* **2004,** *3,* 249-253.
(6) Arcaute, K.; Mann, B.; Wicker, R. *Acta Biomater. 6,* 1047-1054.
(7) Koh, W.-G.; Pishko, M. *Anal. Bioanal. Chem.* **2006,** *385,* 1389-1397.
(8) Liu, V. A.; Bhatia, S. N. *Biomed. Microdevices* **2002,** *4,* 257-266.
(9) Hahn, M.; Miller, J.; West, J. *Adv. Mater.* **2005,** *17,* 2939-2942.
(10) Hahn, M. S.; Taite, L. J.; Moon, J. J.; Rowland, M. C.; Ruffino, K. A.; West, J. L. *Biomaterials* **2006,** *27,* 2519-2524.
(11) Hahn, M. S.; Miller, J. S.; West, J. L. *Adv. Mater.* **2006,** *18,* 2679-2684.
(12) Polizzotti, B. D.; Fairbanks, B. D.; Anseth, K. S. *Biomacromolecules* **2008,** *9,* 1084-1087.
(13) DeForest, C. A.; Polizzotti, B. D.; Anseth, K. S. *Nat. Mater.* **2009,** *8,* 659-664.
(14) Kloxin, A. M.; Kasko, A. M.; Salinas, C. N.; Anseth, K. S. *Science* **2009,** *324,* 59-63.
(15) Maruo, S.; Nakamura, O.; Kawata, S. *Opt. Lett.* **1997,** *22,* 132-134.
(16) Kuebler, S.; Braun, K.; Zhou, W.; Cammack, J.; Yu, T.; Ober, C.; Marder, S.; Perry, J. *J. Photochem. and Photobiol., A* **2003,** 163-170.

For questions, product data, or new product suggestions, please contact Aldrich Materials Science at *matsci@sial.com*.

ALDRICH Materials Science

63

Polyethylene Glycols

For your convenience, we list the polymers using the terms α and ω to refer to the terminal end groups of the polymer.

For a complete list of available PEG and PEO materials, please visit *aldrich.com/poly*

Oligo and Poly(ethylene glycol)

α-end	ω-end	Molecular Weight	Structure	Cat. No.
OH	OH	194.23	HO~O~O~O~OH	110175-5G 110175-100G 110175-1KG 110175-3KG 110175-20KG
OH	OH	238.28	$HOCH_2CH_2(OCH_2CH_2)_4OH$	335754-5G 335754-25G
OH	OH	282.33	H-[O~]$_6$OH	259268-5G 259268-25G
OH	OH	average M_n 300	H-[O~]$_n$OH	202371-5G 202371-250G 202371-500G 202371-1KG 202371-20KG
OH	OH	average M_n 400	H-[O~]$_n$OH	202398-5G 202398-250G 202398-500G 202398-20KG
OH	OH	average M_n 600	H-[O~]$_n$OH	202401-5G 202401-250G 202401-500G 202401-20KG
OH	OH	mol wt range 1400-1600	H-[O~]$_n$OH	81210-1KG 81210-5KG
OH	OH	average M_n 2050	H-[O~]$_n$OH	295906-5G 295906-250G 295906-500G
OH	OH	average M_n 3,350	H-[O~]$_n$OH	202444-250G 202444-500G
OH	OH	average M_n 4,000	H-[O~]$_n$OH	81240-1KG 81240-5KG
OH	OH	average M_n 6,000	H-[O~]$_n$OH	81260-1KG 81260-5KG
OH	OH	average M_v ~8,000	H-[O~]$_n$OH	202452-5G 202452-250G 202452-500G
OH	OH	average M_n 10,000	H-[O~]$_n$OH	309028-250G 309028-500G
OH	OH	average M_n 14,000	H-[O~]$_n$OH	637726-100G 637726-1KG
OH	OH	average M_n 20,000	H-[O~]$_n$OH	81300-1KG 81300-5KG
OH	OH	average M_n 35,000	H-[O~]$_n$OH	81310-1KG 81310-5KG
OH	OH	average M_v 100,000	H-[O~]$_n$OH	181986-5G 181986-250G 181986-500G
OH	OH	average M_v 200,000	H-[O~]$_n$OH	181994-5G 181994-250G 181994-500G
OH	OH	average M_v 400,000	H-[O~]$_n$OH	372773-5G 372773-250G 372773-500G
OH	OH	average M_v 600,000	H-[O~]$_n$OH	182028-5G 182028-250G 182028-500G
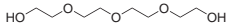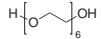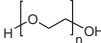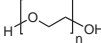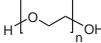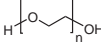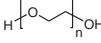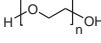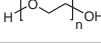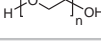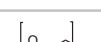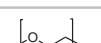
Monofunctional PEGs

α-end	ω-end	Molecular Weight	Structure	Cat. No.
CH$_3$	OH	average M$_n$ 550		202487-5G 202487-250G 202487-500G
CH$_3$	OH	average M$_n$ 750		202495-250G 202495-500G
CH$_3$	OH	average M$_n$ 5,000		81323-250G 81323-1KG
CH$_3$	OH	average M$_w$ 2,000		81321-250G 81321-1KG
CH$_3$	OH	M$_n$ 10,000		732621-5G 732621-25G
CH$_3$	OH	M$_n$ 20,000		732613-5G 732613-25G
CH$_3$	Tosylate	M$_n$ 1,000		729116-5G
CH$_3$	Tosylate	M$_n$ 2,000		729124-5G
CH$_3$	Tosylate	M$_n$ 5,000		729132-5G
CH$_3$	Maleimide	M$_n$ 2,000		731765-1G 731765-5G
CH$_3$	SH	M$_n$ 1,000		729108-1G 729108-5G
CH$_3$	SH	M$_n$ 2,000		729140-1G 729140-5G
CH$_3$	SH	M$_n$ 5,000		729159-1G 729159-5G
CH$_3$	Acetylene	average M$_n$ 2,000		699802-500MG
CH$_3$	Acrylate	average M$_n$ 2,000	n = 8-9	730270-1G
CH$_3$	Acrylate	average M$_n$ 5,000	n = 8-9	730289-1G
CH$_3$	Methacrylate	average M$_n$ 246		409545-250ML 409545-1L
CH$_3$	Methacrylate	average M$_n$ 300		447935-100ML 447935-500ML

For questions, product data, or new product suggestions, please contact Aldrich Materials Science at *matsci@sial.com*.

ALDRICH Materials Science

65

α-end	ω-end	Molecular Weight	Structure	Cat. No.
CH$_3$	Methacrylate	average M$_n$ 475		447943-100ML 447943-500ML
CH$_3$	Methacrylate	average M$_n$ 950		447951-100ML 447951-500ML
CH$_3$	Methacrylate	average M$_n$ 2,000		730319-1G
CH$_3$	Methacrylate	average M$_n$ 5,000		730327-1G

Homobifunctional PEGs

α-end	ω-end	Molecular Weight	Structure	Cat. No.
NH$_2$	NH$_2$	M$_w$ 2,000		14501-250MG 14501-1G
NH$_2$	NH$_2$	M$_w$ 3,000		14502-250MG 14502-1G
NH$_2$	NH$_2$	M$_w$ 6,000		14504-250MG-F 14504-1G-F
NH$_2$	NH$_2$	M$_w$ 10,000		14508-1G
NH$_2$	NH$_2$	M$_w$ 20,000		14509-1G-F
NH$_2$	NH$_2$	M$_n$ ~2,100		452572-1G 452572-5G
COOH	COOH	average M$_n$ 250		406996-100G
COOH	COOH	average M$_n$ 600		407038-250ML 407038-1L
SH	SH	M$_n$ 900-1,100 average M$_n$ 1,000		717142-1G
SH	SH	M$_n$ 1,350-1,650 average M$_n$ 1,500		704369-1G
SH	SH	M$_n$ 3,060-3,740 average M$_n$ 3,400		704539-1G
SH	SH	average M$_n$ 8,000		705004-1G
Tosylate	Tosylate	average M$_n$ 1,300		719080-5G
Tosylate	Tosylate	average M$_n$ 1,800		704458-5G
Tosylate	Tosylate	average M$_n$ 3,500		701750-5G
Tosylate	Tosylate	average M$_n$ 10,000		705047-5G

α-end	ω-end	Molecular Weight	Structure	Cat. No.
Acrylate	Acrylate	average M_n 258		475629-100ML 475629-500ML
Acrylate	Acrylate	average M_n 575		437441-100ML 437441-500ML
Acrylate	Acrylate	average M_n 700		455008-100ML 455008-500ML
Acrylate	Acrylate	average M_n 2,000		701971-1G
Acrylate	Acrylate	average M_n 6,000		701963-1G
Acrylate	Acrylate	average M_n 1,000		729086-1G
Acrylate	Acrylate	average M_n 10,000		729094-1G
Methacrylate	Methacrylate	average M_n 550		409510-250ML 409510-1L
Methacrylate	Methacrylate	average M_n 750		437468-250ML 437468-1L
Methacrylate	Methacrylate	average M_n 2000		687529-1G
Methacrylate	Methacrylate	average M_n 6000		687537-1G
Methacrylate	Methacrylate	average M_n 20,000		725692-1G
Methacrylate	Methacrylate	average M_n 10,000		725684-1G
Acrylamide	Acrylamide	average M_n 3,500		725676-1G
Vinyl	Vinyl	average M_n 240		410195-5ML 410195-25ML
Acetylene	Acetylene	average M_n 2,000		699810-500MG
Glycidyl	Glycidyl	average M_n 526		475696-100ML 475696-500ML

For questions, product data, or new product suggestions, please contact Aldrich Materials Science at *matsci@sial.com*.

67

Conjugated Polymers for the Engineering of Device/Tissue Interface

David C. Martin*, Laura K. Povlich, and Kathleen E. Feldman
Department of Materials Science and Engineering
The University of Delaware
Newark, DE 19716
*Email: milty@udel.edu

Introduction

There is considerable interest in the development of conjugated, electronically and ionically active polymers for interfacing active biomedical devices with living tissue.[1-6] Conjugated polymers offer charge transport between inorganic, electrically conducting metals and organic, proton-conducting biological systems. These materials are potentially useful for a wide variety of bionic devices including cochlear, retinal, and cortical implants, as well as pacemakers and glucose sensors.[7] Candidate materials that have been investigated include polypyrrole (PPy) and functionalized polythiophenes such as poly(3,4-ethylene dioxythiophene) (PEDOT).[8-10] These materials can be deposited directly onto the surface of metal electrodes using an oxidative electrochemical deposition process.[11-13] Although conjugated polymers are not as electrically active as conventional metals, they create a soft, high surface area film that results in a significant reduction in the electrical impedance of biomedical devices in the biologically relevant frequency range (around 1,000 Hz).[12-14] This frequency corresponds to the typical pulse width of a neural signal (around 1–2 msec).[15]

An example microelectronic biomedical device incorporating conducting polymers, namely a silicon-based microfabricated cortical electrode, is schematically shown in **Figure 1a**.[16] The schematic shows an approximately 40 micron diameter PEDOT coating (blue) deposited onto the last electrode site. **Figure 1b** shows the actual image of the electrode with the PEDOT coating (white) on one of the electrode sites. **Figure 1c** is an SEM image of the cross-section of a sample with a ~1 micron thick coating of electrochemically deposited PEDOT prepared in our laboratory at the University of Delaware.
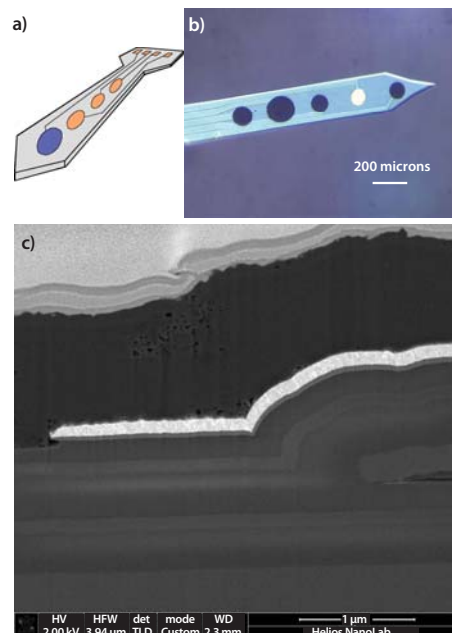
Figure 1. (a) Schematic of a microelectronic biomedical device with integrated conducting polymer coated domains (blue). (b) An actual image of a biomedical electrode with the PEDOT coating (blue) on multiple electrode sites. (c) This cross-sectional SEM image of a biomedical device prepared in our laboratory showing an approximately 1μm thick layer of PEDOT overlaying a metal electrode was obtained on a Helios NanoLab Focused Ion Beam (FIB) instrument at the FEI Laboratory in Hillsboro, OR (fei.com).

PEDOT has been shown to be much more chemically stable than PPy, presumably because the diethoxy substituents replace the extra hydrogen atoms that lead to synthetic defects possible in PPy.[17,18] The electron donating nature of the pendant PEDOT oxygen atoms also improves the conductivity of the molecule. It has been noted that there are striking chemical similarities between PEDOT and melanin, (**Figure 2**) the natural black pigmentation molecule synthesized by most plants and animals.

Conjugated Polymers in Natural Systems
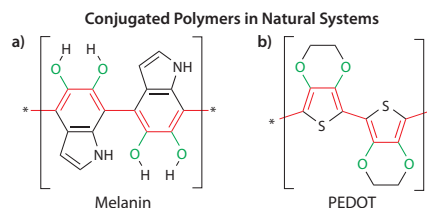
Melanin

PEDOT

Figure 2. (a) The repeat unit of melanin, a natural, conjugated polymer pigment which absorbs UV light due to the conjugated backbone. (b) Synthetic PEDOT polymer with the similarities to melanin highlighted using red and green.

To further improve the performance of molecules such as PEDOT for electronic biomedical device applications, it is necessary to focus additional attention on two critical interfaces: (1) the junction between the solid metal substrate and the conjugated polymer, and (2) the junction between the conjugated polymer and the living tissue. In both cases, it would be useful to have molecules available that could better connect these two different materials. Here, we consider the nature of these material interfaces and describe several monomers that can be used to make functionalized copolymers of particular importance for both of these applications.

Metal-Polymer Interfaces

The mechanical strength and reliability of the conjugated polymer-metal interface are particularly important when designing biomedical devices. The adhesion of the polymer to the metal is a function of the surface treatment of the metal, the method of polymer deposition, and the counter-ion used during the deposition process.[19,20] Molecular designs that could improve the interaction between the polymer and the metal surface are of particular interest, since they would ensure that the polymer coating will be bonded to the substrate as strongly as possible. It is important that any such design maintains efficient charge transport between the metal and the polymer, and eventually, the surrounding electrolyte.

Typical metals used in biomedical devices include gold, platinum-iridium alloys, and stainless steel. The metals are chosen because of their resistance to corrosion and their stability *in vivo*. One method to improve the polymer-metal adhesion is to create a functionalized conjugated monomer that has pendant groups designed to specifically bond with the metal surface of interest.[21] Examples include thiol- or acid-functionalized monomers (**Figure 3**) that could be used to create a thin layer of covalently bonded thiophenes, which could subsequently be reacted to form a thicker layer of a conducting polymer film. The functionalized monomers can also be used selectively at the metal-polymer interface as an adhesion promoter, thereby reducing the total amount of material necessary in the device design.
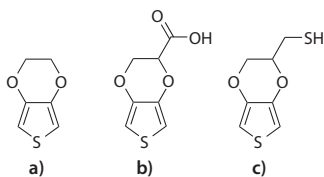
Figure 3. Chemical structures of (**a**) EDOT (Aldrich Prod. No. 483028) and two example monomers that can be used to promote adhesion at the polymer-metal interface: (**b**) EDOT-Acid and (**c**) EDOT-Thiol.

Polymer-Tissue Interfaces

It is possible to design and synthesize functionalized versions of pyrrole and thiophene monomers that can also be electrochemically polymerized.[22] Thin films of functionalized PEDOT with various compositions and precisely controlled aqueous surface wetting angles (from 40–80 degrees) have been prepared using EDOT monomers with alcohol, acid, and amine functionalities.[23] We have developed a carboxylic acid variant of EDOT that has the potential for a wide range of subsequent bio-functionalization opportunities, but its synthesis has proven somewhat difficult to scale up to useful quantities.[21,24] A potentially more robust method involving the use of pendant alkynes capable of azide-alkyne cycloaddition or "click" reactions is illustrated in **Figure 4**.[25-27]
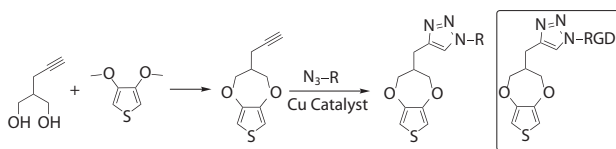
Figure 4. Chemical structure of an alkyne-substituted ProDOT monomer that can be further functionalized using "click" chemistry. An RGD functionalized ProDOT monomer is shown in the box.

At the interface between the conjugated polymer and the tissue, it is also possible to envision functionalized thiophene monomers that can form specific interactions with cells or the extracellular matrix. For example, a thiophene could be functionalized with a biologically active pendant group, such as a peptide sequence known to bind strongly to receptors on cells (**Figure 4**). Examples include the widely studied RGD peptide sequence from fibronectin, or the (Ile-Lys-Val-Ala-Val) IKVAV and Tyr-Ile-Gly-Ser-Arg (YIGSR, Sigma Prod. No. T7154) sequences from laminin.[28-30]

Molecules that are similar to those of natural melanins are also of interest. One example we recently investigated is 5,6-dimethoxyindole-2-carboxylic acid (DMICA), a methoxylated variant of a melanin repeat unit that can be readily deposited using methods similar to those used for PEDOT.[31] The resulting polymer, PDMICA, is crystalline and has an olive-green color not seen in natural melanin. It is also electrochromic, switching from green, to purple, to clear as the voltage is cycled.

Future Opportunities

Functionalized thiophene monomers also offer many opportunities for solution polymerization of novel conjugated polymers with designed structure and properties. Examples include fully soluble conjugated polymers that could be used as fibers or sensors. The ability to create oriented assemblies of these materials through solution spinning or electrospinning should make it possible to understand and optimize their performance in applications.

Acknowledgments

References
(1) Berggren, M.; Richter-Dahlfors, A. *Adv. Mater.* **2007**, *19*, 3201-3213.
(2) Guimard, N. K.; Gomez, N.; Schmidt, C. E. *Prog. Polym. Sci.* **2007**, *32*, 876-921.
(3) Wallace, G. G.; Spinks, G. M. *Soft Matter.* **2007**, *3*, 665-671.
(4) Kotov, N. A.; Winter, J. O.; Clements, I. P.; Jan, E.; Timko, B. P.; Campidelli, S.; Pathak, Sm.; Mazzatenta, A.; Lieber, C. M.; Prato, M.; Bellamkonda, R. V.; Silva, G. A.; Kam, N. W. S.; Patolsky, F.; Ballerini, L. *Adv. Mater.* **2009**, *21*, 3970-4004.
(5) Owens, R. M.; Malliaras, G. G. *MRS Bulletin* **2010**, *35*, 449-456.
(6) Poole-Warren, L.; Lovell, N.; Baek, S.; Green, R. *Expert Rev. Med. Devices* **2010**, *7*, 35-49.
(7) Kim, D.-H.; Richardson-Burns, S. M.; Povlich, L. K.; Abidian, M.; Spanninga, S.; Hendricks, J. L. **2007**, W. M. Reichert (Ed.), *Indwelling Neural Implants: Strategies for Contending with the In-Vivo Environment.* Boca Raton, FL: Taylor and Francis.
(8) Schmidt, C. E.; Shastri, V. R.; Vacanti, J. P.; Langer, R. *Proc. Natl. Acad. Sci. USA* **1997**, *94*, 8948-8953.
(9) Shastri, V. R.; Schmidt, C. E.; Langer, R. S.; Vacanti, J. P. **2000**, *Children's Medical Center Corporation Massachusetts Institute of Technology, USA.*
(10) Xiao, Y.; Cui, X.; Martin, D. C. *J. Electroanal. Chem.* **2004**, *573*, 43-48.
(11) Groenendall, L. B.; Jonas, F.; Freitag, D.; Pielartzik, H.; Reynolds, J. R. *Adv. Mater.* **2000**, *12*, 481-494.
(12) Cui, X.; Hetke, J. F.; Wiler, J. A.; Anderson, D. J.; Martin, D. C. *Sens. Actuators, A* **2001**, *93*, 8-18.
(13) Cui, X.; Lee, V. A.; Raphael, Y.; Wiler, J. A.; Hetke, J. F.; Anderson, D. J. *J. Biomed. Mater. Res.* **2001**, *56*, 261-272.
(14) Yang, J.; Martin, D. C. *J. Mater. Res.* **2006**, *21*, 1124-1132.
(15) Kandel, E. R.; Schwartz, J. H.; Jessell, T. M. **2000**, *Principles of Neural Science.* New York, NY: Mc-Graw-Hill.

For questions, product data, or new product suggestions, please contact Aldrich Materials Science at *matsci@sial.com*.

ALDRICH ® Materials Science

69

(16) Specific examples of such devices can be viewed at *neuronexustech.com*.

(17) Yamato, H.; Ohwa, M.; Wernet, W. *J. Electroanal. Chem.* **1995**, *397*, 163-170.

(18) Cui, X.; Martin, D. C. *Sens. Actuators, B* **2003**, *89*, 92-102.

(19) Cui, X. **2002**, *Surface Modification of Neural Prosthetic Devices by Conducting Polymers and Biopolymers.* The University of Michigan, Ann Arbor, MI

(20) Cui, X.; Martin, D. C. *Sens. Actuators, A* **2003**, *103*, 384-394.

(21) Povlich, L. K.; Cho, J. C.; Spanninga, S.; Martin, D. C.; Kim, J. *Polym. Prepr.* **2007**, *48*, 7-8.

(22) Groenendaal, L. B.; Zotti, G.; Aubert, P.-H.; Waybright, S. M.; Reynolds, J. R. *Adv. Mater.* **2003**, *15*, 855-879.

(23) Luo, S.-C.; Ali, E. M.; Tansil, N. C.; Yu, H.-h.; Gao, S.; Kantchev, E. A. B. *Langmuir* **2008**, *24*, 8071-8077.

(24) Kim, J.; Cho, C.; Povlich, L. K.; Martin, D. C. **2010**, Carboxylic Acid-Modified EDOT for Bioconjugation. U.S. Patent No 7,708, 908 B2. University of Michigan Ref. No. 3540, Harness Dickey & Pierce P.L.C. Ref. No. 2115-2003540/PS1**.** Filed February 28, 2008.

(25) Sahoo, R.; Mishra, S. P.; Kumar, A.; Sindhu, S.; Rao, K. N.; Gopal, E. S. R. *Opt. Mater.* **2007**, *30*, 143-145.

(26) Kumar, A.; Mishra, S. P. **2006**, Novel 3,4-Propylenedioxythiophene Derivatives with Pendant Functional Groups. *Indian Institute of Technology Bombay, India*

(27) Sinha, J.; Sahoo, R.; Kumar, A. *Macromolecules* **2009**, *42*, 2015-2022.

(28) Rouslahti, E. *Annu. Rev. Cell Dev. Biol.* **1966**, *12*, 697-715.

(29) Sephel, T. C.; Tashiro, K.-I.; Sasaki, M.; Greatorex, D.; Martin, G. R.; Yamada, Y.; Kleinman, H. K. *Biochem. Biophys. Res. Commun.* **1989**, *102*, 821-829.

(30) Ranieri, J. P.; Bellamkonda, R.; Bekos, E. J.; Vargo, T. G.; Gardella, J. A.; Aebischer, P. *J. Biomed. Mater. Res.* **1995**, *29*, 779-785.

(31) Povlich, L. K.; Le, J.; Kim, J.; Martin, D. C. *Macromolecules* **2010**, *43*, 3770-3774.

Monomers for Conductive Polymers

Polypyrroles (PPys) have lower oxidation potential compared to polythiophenes, and can be easily deposited on surfaces for applications in batteries, chemical sensors, and ion-selective electrodes. PPy is biocompatible and is commonly used in bio-electrochemistry and biosensor research.

For a complete list of available monomers and polymers for organic electronics applications, please visit *aldrich.com/oel*

Pyrrole Monomers

Name	Structure	Purity	Cat. No.
Pyrrole		98%	131709-25ML 131709-100ML 131709-500ML
1*H*-Pyrrole-1-propionic acid		97%	687545-1G
4-(3-Pyrrolyl)butyric acid		95%	682578-100MG 682578-500MG
11-(1*H*-pyrrol-1-yl)undecane-1-thiol		96%	717223-1G
1-(4-Methylphenyl)-1*H*-pyrrole		97%	452963-5G
1-(4-Methoxyphenyl)-1*H*-pyrrole		97%	452955-1G 452955-5G
1-(4-Nitrophenyl)-1*H*-pyrrole		97%	447358-1G 447358-5G
3,4-Ethylenedioxypyrrole		2 % (w/v) in THF	648310-2ML 648310-10ML
3,4-Propylenedioxypyrrole		2 % (w/v) in THF	648329-2ML 648329-10ML
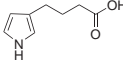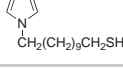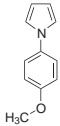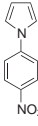
Thiophene Monomers

Name	Structure	Purity	Cat. No.
Thiophene		≥99%	T31801-5G T31801-100G T31801-500G
3,4-Dimethoxythiophene		97%	668257-5G
3,4-Ethylenedioxythiophene		97%	483028-10G
Hydroxymethyl EDOT		95%	687553-500MG
EDOT carboxylic acid		-	729167-500MG
3,4-Propylenedioxythiophene		97%	660485-100MG 660485-500MG
3,4-(2,2-Dimethylpropylenedioxy)thiophene		97%	660523-500MG
3,4-(2',2'-Diethylpropylene)dioxythiophene		97%	669210-250MG
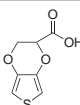
For questions, product data, or new product suggestions, please contact Aldrich Materials Science at *matsci@sial.com*.

ALDRICH Materials Science

Conductive Polymers

Polypyrroles

Name	Structure	Conductivity	Cat. No.
Polypyrrole doped	• X organic acid anion	> 0.0005 S/cm (dried cast film)	482552-100ML
Polypyrrole	• X organic acid anion	0.5-1.5 S/cm (pressed pellet, typical)	578177-10G
Polypyrrole	• X organic acid anion	~ 8.5 S/cm	577065-10G
Polypyrrole	• X organic acid anion	10-40 S/cm	577030-5G 577030-25G
Polypyrrole	• X organic acid anion	30 S/cm (bulk)	530573-25G

Polythiophenes

Name	Structure	Conductivity	Property	Cat. No.
Poly(3,4-ethylenedioxythiophene), bis-poly(ethyleneglycol), lauryl terminated		10-60 S/cm	0.4-0.9 wt. % (content of dispersion)	687316-25G
Poly(3,4-ethylenedioxythiophene), tetramethacrylate end-capped solution		0.1-0.5 S/cm (bulk conductivity)	average M_n ~6,000 ~1,360-1,600 g/mol (methacrylate equivalent weight), 0.5 wt. % (dispersion in nitromethane)	649821-25G
		0.1-0.5 S/cm (bulk conductivity)	average M_n ~6,000 ~1,360-1,600 g/mol (methacrylate equivalent weight)	649813-25G
Poly(3,4-ethylenedioxythiophene)-*block*-poly(ethylene glycol) solution	•Anionic dopant	10^{-4}-10^{-3} S/cm	1 wt. % dispersion in nitromethane	649791-25G
		0.5-3 S/cm (bulk)	1 wt. % dispersion in nitromethane	649805-25G
		0.5-3 S/cm (bulk)	1 wt. % dispersion in propylene carbonate	649783-25G
Poly(3,4-ethylenedioxythiophene)-poly(styrenesulfonate)		~ 1E-5 S/cm	2.8 wt. % dispersion in H_2O	560596-25G 560596-100G
		1 S/cm	1.3 wt % dispersion in H_2O	483095-250G
		150 S/cm (18 μm film thickness)	2.2-2.6% in H_2O	655201-5G 655201-25G
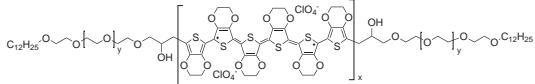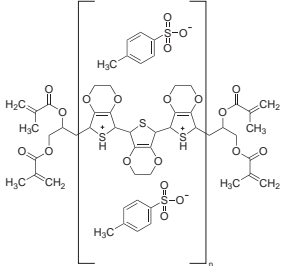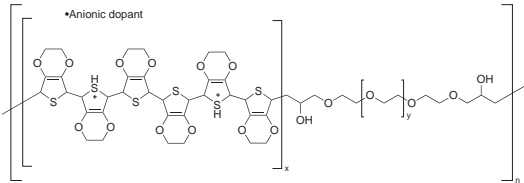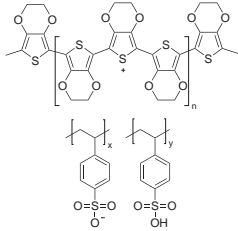
The Progress in Development of Dental Restorative Materials

Jeffrey Stansbury[1]* and Christopher Bowman[2]
[1]Department of Chemical and Biological Engineering Department of Craniofacial Biology, School of Dental Medicine, University of Colorado Boulder, CO 80045-0508
[2]Department of Chemical and Biological Engineering, University of Colorado Boulder, CO 80309-0424
*Email: jeffrey.stansbury@colorado.edu

Introduction

With dentists placing nearly 100 million dental fillings into patients' teeth annually in the U.S. alone, polymeric composite restoratives account for a very large share of the biomaterials market. These pigmented materials are composed mainly of liquid monomers and surface-functionalized particulate inorganic fillers, and can, upon polymerization, indistinguishably mimic the appearance of a natural tooth. While this natural appearance appeals to patients, the ability of the composites to bond to both dentin and enamel also makes polymeric composites a practical alternative to amalgam-based restorative materials. The matrix phase of currently used dental composites is predominantly based on dimethacrylate monomers. An excellent example of a commonly used bulky aromatic dimethacrylate monomer is 2,2-bis[p-(2'-hydroxy-3'-methacryloxypropoxy)phenyl]pro-pane (BisGMA) (Aldrich Prod. No. 494356), which was originally developed by Bowen specifically for dental composite applications.[1]

The bulky BisGMA monomer, which is extremely viscous due to strong intermolecular hydrogen bonding interactions, is normally used with lower viscosity comonomers such as urethane dimethacrylate (Aldrich Prod. No. 436909), ethoxylated bisphenol A dimethacrylate (BisEMA, Aldrich Prod. No. 455059) and triethylene glycol dimethacrylate (TEGDMA, Aldrich Prod. No. 261548) among others.[2] Efficient, rapid photopolymerization is typically achieved with visible light (wavelength 400–500 nm) using a suitable radical photoinitiator such as camphor-quinone (Aldrich Prod. No. 124893) along with a tertiary amine photoreductant such as ethyl dimethylaminobenzoate (Aldrich Prod. No. E24905) or 2-(dimethylamino)ethyl methacrylate (Aldrich Prod. No. 234907).[3-5] Other initiating systems have also been reported, including bisacylphosphine oxides, titanocenes and germanium-based compounds.[6,7]

Composite Restorative Materials

The glass-ceramic fillers in dental composites are typically aluminosilicate-based, with the inclusion of heavy metal oxides such as barium, strontium or zirconium to contribute X-ray opacity.[8] The filler particle dimensions vary from approximately 0.1–10 μm for ground glass, to around 20–50 nm for pyrolytic or sol-gel derived silica and other nanomaterials. Organosilanes, mainly methacryloxypropyltrimethoxysilane (Aldrich Prod. No. 440159), are used as coupling agents to provide the essential covalent connection between the filler and the polymer matrix. A combination of multiple filler particle sizes as well as silane surface treatment are used to incorporate a significant proportion (70–90 weight % or 30–55 volume %) of the high modulus reinforcing filler into the resin matrix (Figure 1). The high filler content in dental composites provides increased modulus, strength, abrasion resistance and toughness, as well as reduced thermal expansion. The filler

component also limits the polymerization shrinkage associated with the transition of the liquid monomers to a highly cross-linked glassy polymer matrix. This *in situ* polymerization is necessary to achieve a restoration that is well adapted to the surrounding tooth structure.
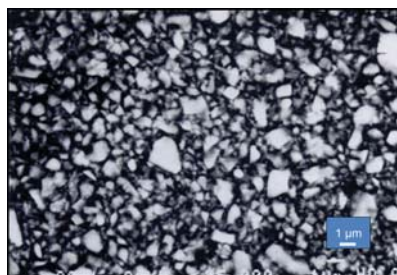
Figure 1. Scanning electron micrograph of a polished dental composite showing the irregularly sized inorganic particles embedded into a polymer matrix.

The intraoral placement restricts the photopolymerization conditions that can be employed to cure the restoratives, making the selection of materials significantly challenging. This unique placement has necessitated the development of ambient temperature, rapid, high conversion polymerization reactions that lead to high performance, aesthetic composite materials. The resulting restorative materials must be able to withstand substantial masticatory cyclic stresses (chewing stresses), as well as exposure to an aqueous environment involving temperature variations resulting from food and drink consumption. The critical adhesion of the composite to a tooth is reliant on an acid etch of dentin and enamel that demineralizes the surface and allows for strong micromechanical interlocking with a polymerizable adhesive layer.[9] This layer serves as a transition from the relatively hydrophilic dentin within the tooth to the much more hydrophobic restorative composite.

Shrinkage and Stress in Restorative Composites

When bonded interfaces are imposed on a polymerizing sample of a composite, as is necessary with a dental restoration, the resultant restriction in free shrinkage induces significant internal and external stress (Figure 2a). This stress can cause a series of problems including: (a) deflection of the tooth, (b) failure of sections of the adhesive bond, and (c) defect formation within the polymer matrix at the filler-matrix interface, or in the adjacent enamel substrate.[10] Reliable, long-term stability of the tooth-restoration interface has remained elusive, prompting substantial new materials research and development projects in both industrial and academic laboratories. The concerns with polymerization shrinkage and stress are not unique to dental polymers, and the research can also be applied to other industrial polymer applications including coatings, adhesives, encapsulants, aspheric lenses and photolithography.

Stress is defined as a product of strain and modulus ($\sigma = \varepsilon \times E$), where σ is the stress, ε is the strain, and E is Young's Modulus. Stress development during the formation of glassy polymers in a polymerizing composite is a major concern. Therefore a basic understanding of the evolution of shrinkage strain and elastic modulus is critical to begin solving the stress/strain problems. The values of the shrinkage strain and modulus are dependent on the degree polymerization, along with temperature change in the non-isothermal composite photopolymerizations. Dimethacrylate monomers are capable of forming polymer networks with glass transition temperatures above the curing temperature, but this usually means that a significant percentage of the methacrylate functionality remains un-reacted in the fully cured polymer.[11]

For questions, product data, or new product suggestions, please contact Aldrich Materials Science at *matsci@sial.com*.

73
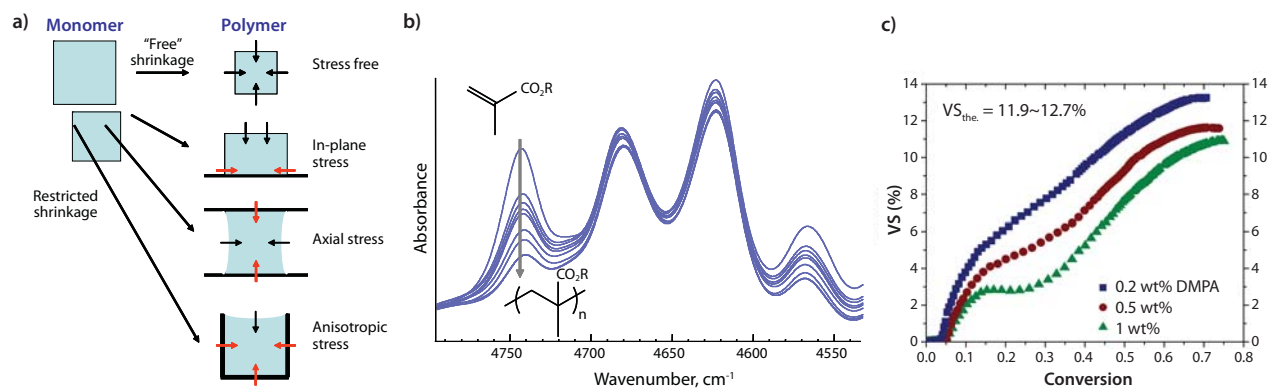
Figure 2. (a). Restricted shrinkage associated with bonded surfaces during polymerization leads to significant stress development within a polymerizing sample. (b) Near-infrared spectroscopy focused on the methacrylate =CH₂ combination band can be used to monitor reaction kinetics and conversion of BisGMA/TEGDMA monomers during polymerization. The grey arrow at 4745 cm⁻¹ indicates the consumption of monomer, showing the progress of the polymerization reaction. (c) Non-linear dynamic volumetric polymerization shrinkage (VS) of TEGDMA photoinitiated with various concentrations of 2,2-dimethoxy-2-phenylacetophenone (DMPA, Aldrich Prod. No. 196118) as a function of conversion, demonstrating thermal expansion/contraction effects and delayed shrinkage in the glassy state. From the graph, the glassy state begins at approximately 0.45 conversion of monomer.

During the photopolymerization, a liquid monomer converts to a crosslinked polymer by passing through the stages of gelation, rubbery regime and vitrification (transition into a glassy state) as a function of the monomer to polymer conversion progress. A series of hybrid analytical techniques have been developed that employ real-time near-infrared spectroscopy to monitor the polymerization reaction rate and conversion simultaneously with dynamic measurements of volumetric shrinkage, modulus or stress during the photopolymerization process (**Figure 2b**).[10,12] These studies have demonstrated that shrinkage is nonlinear with respect to conversion due to both thermal excursions during polymerization and a reduced rate of shrinkage relative to conversion in the glassy polymeric state. Modulus and stress development were found to be concentrated in the later stages of conversion and at the onset of vitrification (**Figure 2c**). Based on this information, and on the assumption that stress reduction should not be accomplished by limiting either conversion or modulus of the polymer, there are several modern approaches with practical potential to produce lower stress dental polymers.

Designing Bulky Monomers

One possible solution to the polymerization shrinkage problem is the development of new monomers and reactive oligomers that are customized for dental composite applications. A decrease in the initial reactive group concentration generally results in a reduced modulus, but also results in a lower crosslinking density within the polymer network. This unintended consequence may be avoided, for example, by designing a large monomer with a lower initial reactive group concentration, but with an auxiliary reinforcement mechanism to counter the lower covalent crosslink density.

Materials based on the relatively large BisGMA monomer demonstrate anomalously high mechanical strength despite their relatively low limiting conversion and crosslinking density values, most likely as a consequence of hydrogen bonding between the hydoxy and carbonyl groups. This larger monomer strategy, combining physical and covalent crosslinking, is also used in significantly higher molecular weight dimethacrylate monomer analogs of BisGMA, such as the di-*tert* butyl phenol and methacrylic acid substituted monomers synthesized from bisphenol A diglycidyl ether (**Figure 3a**).[13] In the case of the bis(di-*tert*-butylphenoxy)-modified dimethacrylate (DtBP-BisGMA), the steric interactions of the added bulky aromatic groups provide additional physical network reinforcement, allowing low shrinkage and high modulus to be collaboratively maintained.
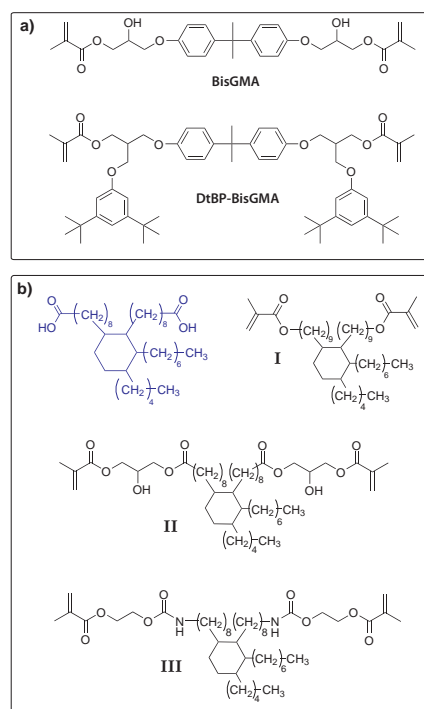
Figure 3. (a) BisGMA (MW = 513) is a representative dimethacrylate monomer commonly used as a co-monomer to form the highly cross-linked polymeric matrix phase in dental composites. The related DtBP-BisGMA (MW = 899) bulkier monomer structure provides polymers with lower polymerization shrinkage and reduced covalent crosslink densities, while maintaining good strength due to physical network reinforcement by the bulky substituent groups. (b) Dimethacrylate monomers based on the C₃₆ diacid core structure (blue). Monomer **I** was prepared by reduction of the diacid to the diol followed by a reaction with methacrylic anhydride. Monomer **II** was synthesized using a diepoxide analog of the core structure and reacting it with methacrylic acid, while monomer **III** was synthesized by the reaction of a diisocyanate analog with 2-hydroxyethyl methacrylate (Aldrich Prod. No. 477028). As co-monomers with selected conventional dimethacrylates, these monomers lead to polymerization-induced phase separation that contributes to lowering of the shrinkage, translating into a reduction in stress.

Copolymer Development

In a different application of bulky monomers to lower polymerization shrinkage, a series of dimethacrylate compounds were prepared from a C_{36} diacid core structure, which results in completely amorphous cured polymers (**Figure 3b**). Beginning with the C_{36} diacid or the corresponding diepoxide, several monomers have been prepared with different connecting groups between the terminal methacrylate groups and the C_{36} core.[14] All these materials produce homopolymers that exhibited very high conversions, along with low shrinkage and extreme hydrophobicity, while remaining rubbery and low modulus at room temperature. When combined as co-monomers with other conventional dental monomers, it was noted that C_{36} diacid monomers lack the ability to hydrogen bond, and showed limited affinity for hydrogen bonding with monomers such as BisGMA. Conversely, the introduction of a hydrogen bonding -OH group into the C_{36} diacid monomer structure imparted compatibility with BisGMA, but not with the ethoxy analog, BisEMA. This limited thermodynamic compatibility can be adjusted based on the binary or ternary co-monomer compositions such that initially homogeneous monomer mixtures produce copolymers with controlled degrees of heterogeneity.

Despite high conversion in the final heterogenous polymers, exceptionally low polymerization shrinkage can be obtained under specific conditions of relative reaction kinetics within the separate phases, and the overall phase structure in the polymerized copolymer material. These heterogeneous copolymer materials demonstrate the potential for late-stage shrinkage recovery, and thus stress relaxation, due to the concentration of stress development toward the very end of the polymerization reaction. Thermoplastic prepolymer additives, so-called low-profile additives, have also been shown to control shrinkage based on internal stress relief at phase boundaries created during the polymerization-induced phase separation.

Preparation of Nanogels

Highly branched, short-chain nanogels have been prepared from relatively concentrated monovinyl/divinyl polymerizations involving solutions of isobornyl methacrylate (Aldrich Prod. No. 392111) and urethane dimethacrylate (**Figure 4**).[15] The discrete globular polymeric nanogel particles have sizes between 5 and 100 nm with molecular weights of 10^4 to more than 10^6 Da. These methacrylate functionalized nanogel particles can be added to dental resins at concentrations up to 50 wt. %, with at least proportional reduction in polymerization shrinkage and stress development. There is also little to no effect on the curing reaction kinetics, conversion, and mechanical strength properties. At levels up to about 20 wt. % of the nanogel, there is only a limited effect on monomer viscosity. Even at very high nanogel loading levels, high amounts of inorganic filler can still be incorporated to give low shrinkage, low stress dental composite materials.
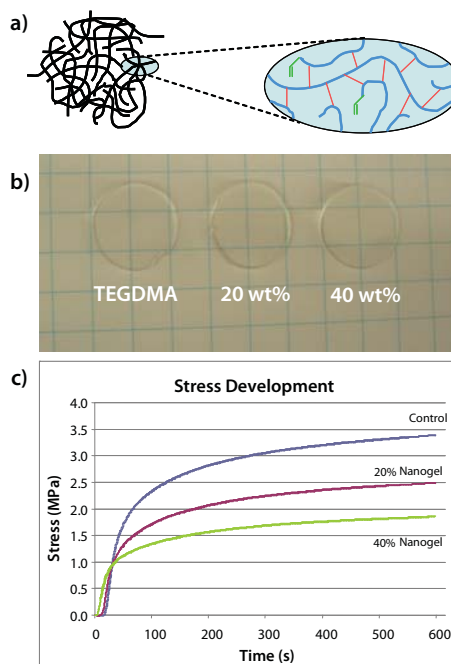
Figure 4. (a) Branched/cyclized nanogel particles can be made from solution copolymerization of monovinyl and divinyl monomers (2:1 molar ratio) with a chain transfer agent used to control chain length, avoid macrogelation, and provide a site to reintroduce reactive methacrylate groups. (b) Even at high concentrations, reactive nanogel particles dispersed in TEGDMA (Aldrich Prod. No. 261548) provide near-optically transparent monomeric and polymeric materials. (c) The polymerization shrinkage and stress are significantly reduced, without detrimental reduction of monomer conversion or mechanical properties[15] in the final nanogel-modified polymer.

For questions, product data, or new product suggestions, please contact Aldrich Materials Science at *matsci@sial.com*.

ALDRICH
Materials Science

75

Methacrylate Cross-Linked Networks Using Thiol-ene Chemistry

There are also methods to reduce polymerization stress that are relatively independent of the shrinkage generated during the curing process. Rather than relying exclusively on free radical chain growth polymerization of methacrylates, a radical-induced thiol-ene polymerization involves a step growth mechanism. Molecules with multiple thiol groups, such as pentaerythritol tetramercaptoproprionate (Aldrich Prod. No. 381462), can be photoinitiated and reacted with compounds containing multiple alkene groups, such as triallyl-1,3,5-triazine-2,4,6-trione (Aldrich Prod. No. 114235), to yield extremely high conversions and highly homogeneous polymer networks.[16,17] Another advantage is that these thiol-ene polymerizations provide well-controlled gel points, which occur at much higher conversions than those of dimethacrylate polymerizations. This is important since shrinkage prior to gelation is accommodated by viscous flow with virtually no stress development within the sample. Therefore, thiol-ene polymerizations with gel points between 40 and >70% conversion are possible based on the step growth reaction process, translating into polymers with dramatically reduced final stress levels compared with polymers made by dimethacrylate polymerization.

In a thiol-ene polymerization, the alkene is typically selected to eliminate or minimize homopolymerization of the -ene component. In this regard, alkenes based on vinyl ethers, vinyl esters, allyl ethers and norbornene functional groups are well suited to maintain a stoichiometric consumption rate with the thiol groups. Mixed thiol-ene/methacrylate resin systems that polymerize through a hybrid step/chain-growth mechanism provide advantages in terms of improved shelf-life stability and enhanced mechanical strength, while still resulting in low stress polymers.[18] On the one hand, as explained above, thiol-alkene reactions are able to generate step-growth networks with very high crosslink densities. On the other hand, thiols are well known to function as effective chain transfer agents with methacrylate monomers. In a simple thiol-modified dimethacrylate photopolymerization, methyl mercaptopropionate (Aldrich Prod. No. 108987) and benzenethiol (Aldrich Prod. No. 240249) demonstrate well-controlled delayed gelation and vitrification leading to a higher final polymeric conversion and modulus, but with significantly reduced stress.[18]

A completely different approach to alleviate stress in polymer networks was recently demonstrated for thiol-ene systems, and is also applicable to crosslinked dimethacrylate materials. This novel approach involves creation of a covalent adaptable network in which the bond structure of the network remains covalent, yet each individual bond can be broken and reformed in the presence of active radical species.[19] In a dental materials application, this approach can be achieved by incorporating allyl sulfide moieties into multifunctional monomers that subsequently undergo a thiol-ene photopolymerization. As polymerization proceeds, addition-fragmentation of the allyl sulfide linkages allows the developing polymer network to relax stress throughout the polymerization rather than simply prior to gelation (**Figure 5**). This adaptive network process has been shown to result in polymerization shrinkage stress reduction of up to 75% when compared with the otherwise identical system of crosslinking monomers with the allyl sulfide group replaced by a propyl sulfide analog.
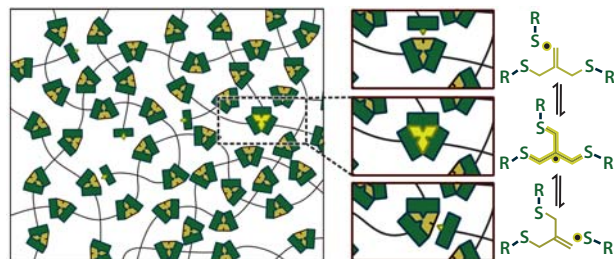
Figure 5. Covalent adaptable network structure based on crosslink units with allyl sulfide groups capable of radical addition-fragmentation to relieve stress during the polymerization. The presence of additional thiol terminated polymer chains allows for the reversible random replacement of existing carbon-sulfur linkages leading to the dissipation of stress throughout the cross-linked polymer network.

Conclusions

Composite materials based on methacrylate monomers are commonly used to provide aesthetic and functional restoration of dental tissue. A broad spectrum of new polymerization chemistries is being developed to further improve the reliability of these materials. Approaches under investigation include the design of new monomers and the use of novel polymerization mechanisms. These approaches are directed toward addressing the ongoing challenges associated with shrinkage during polymerization and stress within the restorative composites, but can also be applied to other industrial polymers.

References
(1) Bowen, R. L. Dental filling material comprising vinyl silane treated fused silica and a binder consisting of the reaction product of bisphenol and glycidyl acrylate. U.S. Patent 3066112, November 27, 1962.
(2) Trujillo-Lemon, M.; Jones, M. S.; Stansbury, J. W. *J. Biomed. Mater. Res., A* **2007**, *83A*, 734-746.
(3) Dickens, S. H.; Stansbury, J. W.; Choi, K. M.; Floyd, C. J. E. *Macromolecules* **2003**, *36*, 6043-6053.
(4) Lovell, L. G.; Berchtold, K. A.; Elliott, J. E.; Lu, H.; Bowman, C. N. *Polym. Adv. Technol.* **2001**, *12*, 335-345.
(5) Stansbury, J.; Dickens, S. *Dent. Mater.* **2001**, *17*, 71-79.
(6) Cook, W. D. *Polymer* **1992**, *33*, 600-609.
(7) Moszner, N.; Fischer, U. K; Ganster, B.; Liska, R.; Rheinberger. V. *Dent. Mater.* **2008**, *24*, 901-907.
(8) Klapdohr, S; Moszner, N. *Monatsh. Chem.* **2005**, *136*, 21-45.
(9) Moszner, N.; Salz, U. *Macromol. Mater. Eng.* **2007**, *292*, 245-271.
(10) Stansbury, J. W.; Trujillo-Lemon, M.; Lu, H.; Ding, X.; Lin, Y.; Ge, J. *Dent. Mater.* **2005**, *21*, 56-67.
(11) Lu, H.; Lovell, L. G.; Bowman, C. N. *Macromolecules* **2001**, *34*, 8021-8025.
(12) Lu, H.; Stansbury, J. W.; Dickens, S. H.; Eichmiller, F. C.; Bowman, C. N. *J. Biomed. Mater. Res., B* **2004**, *71B*, 206-213.
(13) Ge, J. H.; Trujillo, M.; Stansbury, J. *Dent. Mater.* **2005**, *21*, 1163-1169.
(14) Trujillo-Lemon, M.; Ge, J.; Lu, H.; Tanaka, J.; Stansbury, J. W. *J. Polym. Sci., Part A: Polym. Chem.* **2006**, *44*, 3921-3929.
(15) Stansbury, J. W.; Trujillo-Lemon, M.; Ding, X. *Am. Chem. Soc.* Polymer Preprints, **2006**, *47*, 825-826.
(16) Carioscia, J. A.; Schneidewind, L.; O'Brien, C.; Ely, R; Feeser, C.; Cramer, N.; Bowman, C. N. *J. Polym. Sci., Part A: Polym. Chem.* **2007**, *45*, 5686-5696.
(17) Lu, H.; Carioscia, J. A.; Stansbury, J. W.; Bowman, C. N. *Dent. Mater.* **2005**, *21*, 1129-1136.
(18) Cramer, N. B. Couch, C. L.; Schreck, K. M.; Carioscia, J. A.; Boulden, J. E.; Stansbury, J. W.; Bowman, C. N. *Dent. Mater.* **2010**, *26*, 21-28.
(19) Fairbanks, B. D.; Sims, E. S.; Anseth, K. S.; Bowman, C. N. *Macromolecules* **2010**, *43*, 4113-4119.
(20) Kloxin, C. J. Scott, T. F.; Adzima, B. J.; Bowman, C. N. *Macromolecules* **2010**, *43*, 2643-2653.

Methacrylate Monomers

For a complete list of available methacrylate and methacrylamide monomers, please visit *aldrich.com/monomers*

Name	Structure	Purity	Cat. No.
2-Methacryloyloxyethyl phosphorylcholine		*	730114-5G
Morpholinoethyl methacrylate		*	729833-25G
Triphenylmethyl methacrylate		*	730122-5G
Methacrylic acid *N*-hydroxysuccinimide ester		*	730300-5G
2-(Diisopropylamino)ethyl methacrylate		*	730971-25G
2-Hydroxyethyl methacrylate		97%	128635-5G 128635-500G 128635-1KG 128635-18KG
2-Hydroxyethyl methacrylate		≥99%	477028-25ML 477028-100ML
Ethyl methacrylate		99%	234893-100ML 234893-500ML 234893-1L
Glycidyl methacrylate		97%	151238-100G 151238-500G
2-Aminoethyl methacrylate hydrochloride		90%	516155-5G 516155-25G
Lauryl methacrylate		96%	291811-100ML 291811-500ML
Allyl methacrylate		98%	234931-100ML 234931-500ML
3-Sulfopropyl methacrylate potassium salt		98%	251658-100G 251658-500G
Hexyl methacrylate		98%	462373-500G 462373-1KG
Stearyl methacrylate		technical grade	411442-250ML 411442-1L
2-(Diethylamino)ethyl methacrylate		99%	408980-250ML 408980-1L
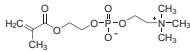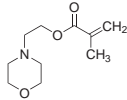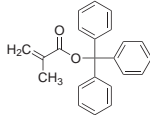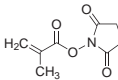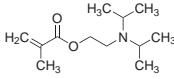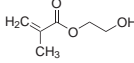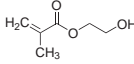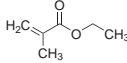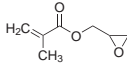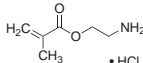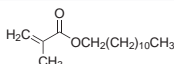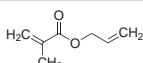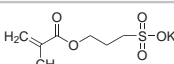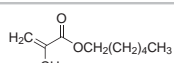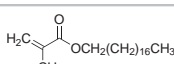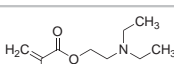
*For updated purities, please visit the Sigma-Aldrich website at *sigma-aldrich.com*

For questions, product data, or new product suggestions, please contact Aldrich Materials Science at *matsci@sial.com*.

ALDRICH Materials Science

77

Methacrylamide Monomers

Name	Structure	Purity	Cat. No.
Methacrylamide		98%	109606-5G 109606-250G 109606-500G
N-Isopropylmethacrylamide		97%	423548-25G
N-[3-(Dimethylamino)propyl]methacrylamide		99%	409472-250ML 409472-1L
N-(3-Aminopropyl)methacrylamide hydrochloride		*	731099-1G 731099-5G
N-Diphenylmethylacrylamide		*	731145-5G
N-(Triphenylmethyl)methacrylamide		*	731781-1G 731781-5G

*For updated purities, please visit the Sigma-Aldrich website at sigma-aldrich.com

Cross-Linkers

Acrylic Cross-Linkers

Name	Structure	Purity/M_n	Cat. No.
N,N'-Hexamethylenebis(methacrylamide)		–	729825-5G
Di(ethylene glycol) dimethacrylate		95%	409006-250ML
Ethylene glycol diacrylate		90%	480797-5ML 480797-25ML
Ethylene glycol dimethacrylate		98%	335681-5ML 335681-100ML 335681-500ML
Triethylene glycol dimethacrylate		95%	261548-250ML 261548-1L
Poly(ethylene glycol) diacrylate		average M_n 575	437441-100ML 437441-500ML
Poly(ethylene glycol) diacrylate		average M_n 700	455008-100ML 455008-500ML
Poly(ethylene glycol) dimethacrylate		average M_n 550	409510-250ML 409510-1L
Poly(ethylene glycol) dimethacrylate		average M_n 750	437468-250ML 437468-1L
N,N'-(1,2-Dihydroxyethylene)bisacrylamide		97%	294381-5G 294381-25G

Thiol Cross-Linkers

Name	Structure	Purity	Cat. No.
1,2-Ethanedithiol	$HSCH_2CH_2SH$	≥90%	398020-100ML 398020-500ML
1,3-Propanedithiol	HS⌒⌒SH	99%	P50609-5G P50609-25G
1,4-Butanedithiol	$HSCH_2CH_2CH_2CH_2SH$	97%	B85404-5G B85404-25G
2,3-Butanedithiol	H_3C⌒CH₃ (SH, SH)	≥97%	264695-1G 264695-5G
1,5-Pentanedithiol	$HSCH_2(CH_2)_3CH_2SH$	96%	242551-5G
2,2′-(Ethylenedioxy)diethanethiol	HS⌒O⌒O⌒SH	95%	465178-100ML 465178-500ML
1,6-Hexanedithiol	$SHCH_2(CH_2)_4CH_2SH$	96%	H12005-5G H12005-25G
1,6-Hexanedithiol	$SHCH_2(CH_2)_4CH_2SH$	99.5%	725382-1G
1,8-Octanedithiol	$HSCH_2(CH_2)_6CH_2SH$	≥97%	O3605-1G O3605-5G
1,9-Nonanedithiol	$HSCH_2(CH_2)_7CH_2SH$	95%	N29805-5G N29805-25G
1,11-Undecanedithiol	$HSCH_2(CH_2)_9CH_2SH$	99%	674281-250MG
5,5′-Bis(mercaptomethyl)-2,2′-bipyridine	HS⌒(pyridine-pyridine)⌒SH	96%	711241-500MG
1,16-Hexadecanedithiol	$HSCH_2(CH_2)_{14}CH_2SH$	99%	674400-100MG

Vinyl Cross-Linkers

Name	Structure	Purity/M_n	Cat. No.
1,4-Butanediol divinyl ether	H_2C═⌒O⌒⌒O⌒═CH_2	98%	123315-10ML 123315-50ML
1,4-Cyclohexanedimethanol divinyl ether, mixture of isomers	H_2C═⌒O⌒(cyclohexane)⌒O⌒═CH_2	98%	406171-100ML 406171-500ML
Di(ethylene glycol) divinyl ether	H_2C═⌒O⌒O⌒O⌒═CH_2	99%	139548-50ML
Poly(ethylene glycol) divinyl ether	H_2C═[⌒O⌒]ₙ O⌒═CH_2	average M_n 240	410195-5ML 410195-25ML
Tri(ethylene glycol) divinyl ether	H_2C═[⌒O⌒]₃ O⌒═CH_2	98%	329800-250ML 329800-1L
1,4-Bis(4-vinylphenoxy)butane	H_2C═⌒(phenyl)⌒O⌒⌒O⌒(phenyl)⌒═CH_2	>90%	730262-1G

For questions, product data, or new product suggestions, please contact Aldrich Materials Science at *matsci@sial.com*.

79

Photoinitiators

Blends of photoinitiators are often used to get the best total cure, cure speed, and minimal color formation. Dyes are used as sensitizers with photoinitiators to shift absorption wavelengths into the near UV and the visible regions. Combinations of dyes and photoinitiators can be selected such that absorption peaks are obtained throughout the entire visible spectrum, allowing the use of visible emission lasers to initiate photopolymerization.

For a complete list of available polymerization photoinitiators, please visit *aldrich.com/polyinitiator*

Name	Structure	Purity	Cat. No.
Acetophenone		99%	A10701-5G A10701-100G A10701-1KG A10701-3KG
Anthraquinone		97%	A90004-500MG A90004-50G A90004-250G
Anthraquinone-2-sulfonic acid sodium salt		97%	123242-100G 123242-1KG
Benzoin		≥99.5%	399396-5G
Benzoin methyl ether		96%	B8703-100G
4,4′-Bis(diethylamino)benzophenone		≥99%	160326-25G 160326-100G
Camphorquinone		97%	124893-5G 124893-10G 124893-50G
2,2-Diethoxyacetophenone		>95%	227102-500G
4,4′-Dihydroxybenzophenone		99%	D110507-5G D110507-25G
2,2-Dimethoxy-2-phenylacetophenone		99%	196118-50G 196118-250G
4′-Ethoxyacetophenone		98%	275719-25G 275719-100G
1-Hydroxycyclohexyl phenyl ketone		99%	405612-50G 405612-250G
2-Hydroxy-2-methylpropiophenone		97%	405655-50ML 405655-250ML
Methyl benzoylformate		98%	M30507-5G M30507-25G
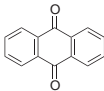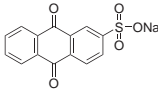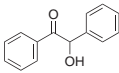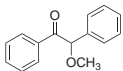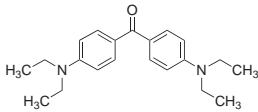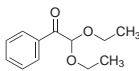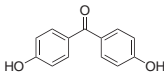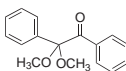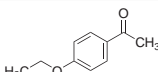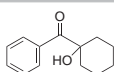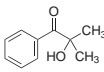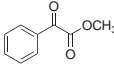
Name	Structure	Purity	Cat. No.
9,10-Phenanthrenequinone		≥99%	156507-5G 156507-25G
Thioxanthen-9-one		97%	T34002-25G T34002-100G
Triarylsulfonium hexafluorophosphate salts, mixed		50% in propylene carbonate	407216-25ML 407216-100ML

Amine Coinitiators

Tertiary amines are commonly used as coinitiators with Norrish Type II organic photoinitiators. The most frequently used free and copolymerizable amines are listed. For a complete list, please visit *aldrich.com/polyinitiator*

Name	Structure	Purity	Cat. No.
2-(Diethylamino)ethyl acrylate		95%	408972-100ML
2-(Diethylamino)ethyl methacrylate		99%	408980-250ML 408980-1L
2-(Dimethylamino)ethyl acrylate		98%	330957-100ML 330957-500ML
4,4'-Bis(diethylamino)benzophenone		≥99%	160326-25G 160326-100G
Ethyl 4-(dimethylamino)benzoate		≥99%	E24905-5G E24905-100G E24905-500G
Michler's ketone		98%	147834-5G 147834-100G 147834-500G

For questions, product data, or new product suggestions, please contact Aldrich Materials Science at *matsci@sial.com*.

81

Strategy for Toxicity Screening of Nanomaterials

Tian Xia,[1,2] Huan Meng,[1,2,†] Saji George,[1,2,†] Haiyuan Zhang,[1,2,†] Xiang Wang,[1,2,†] Zhaoxia Ji,[2,†] Jeffrey I. Zink,[2,3] Andre E. Nel[1,2*]

[1]Division of NanoMedicine, Department of Medicine, University of California, Los Angeles, CA 90095
[2]California NanoSystems Institute, University of California, Los Angeles, CA 90095
[3]Department of Chemistry & Biochemistry, University of California, Los Angeles, CA 90095
*Email: anel@mednet.ucla.edu
[†]Not pictured

Introduction

A key challenge for nanomaterial safety assessment is the ability to handle the large number of newly engineered nanomaterials (ENMs), including developing cost-effective methods that can be used for hazard screening.[1] In order to develop an appropriate screening platform, it is necessary to assemble and synthesize nanomaterial libraries that can be used to screen for specific material compositions and properties that may lead to the generation of a biological hazard.[1-3] Our opinion is that screening using rapid assessment platforms should initially take place at the biomolecular and cellular level to generate a comprehensive database of potentially hazardous events at the nano-bio interface, and then, using these property-activity relationships, to prioritize animal studies that can validate the real-life significance of the *in vitro* observations.[4] Both the National Toxicology Program as well as the National Research Council (NRC) in the US National Academy of Sciences (NAS) have recommended that toxicological testing in the 21st-century evolve from a predominantly descriptive science in animal models to a predictive scientific discipline premised on target-specific, mechanism-based biological screening.[5,6] It was further recommended that biological testing should be based on robust scientific paradigms that can be used to concurrently screen multiple toxicants, rather than costly animal experiments that examine one toxicant at a time.[4,7]

We refer to the above approach as a predictive toxicological paradigm, which can be defined as assessing the *in vivo* toxic potential of a material or substance based on *in vitro* and *in silico* methods.[4] There are four major requirements to keep in mind when establishing this paradigm. The first is to acquire or synthesize compositional and combinatorial ENM libraries that can be used for knowledge generation of the material properties that may lead to biological injury. The second requirement is to develop *in vitro* cellular screening assays that utilize mechanisms and pathways of injury. Third, is to develop high content or rapid throughput screening platforms that are capable of assessing the large number of material compositions and properties, and are based on the pathways of injury. Finally, the *in vitro* data should be used for *in silico* modeling to establish quantitative structure-activity relationships (QSARs) and to generate a hazard ranking that can be used to prioritize animal experiments.

Construction of ENM Libraries

The acquisition and characterization of standard reference nanomaterial (SRM) libraries forms the basic infrastructure requirement that is necessary to screen for toxicity and to elucidate the material properties that are most likely to result in biological injury.[8] The selection of the library materials should take into consideration the commercial production volumes of the different nanomaterials, incorporating the major current ENM classes of materials (metals, metal oxides, silica, and carbon based nanomaterials). The choice of materials should also consider the exposure potential, route of exposure and delivery pathway. For example, free nanoparticles or powders are more likely to become airborne with the potential to generate pulmonary toxicity after inhalation. Thus, it is appropriate to investigate this scenario using lung cells (*in vitro*) and pulmonary exposure (*in vivo*) that ideally should be linked in terms of mechanisms of potential injury. Ideal ENM libraries should also include positive and negative control ENMs to provide a reference point for the evaluation of material toxicity.

As an example of this type of exercise, we began our studies by selecting and synthesizing three metal oxides (TiO_2, CeO_2, and ZnO) as a simple compositional ENM library.[9,10] After establishing valid testing procedures and protocols, we extended the work to include additional metal and metal oxide nanomaterials such as Au, Ag, Pt, SiO_2, Al_2O_3, Fe_3O_4, and quantum dots (**Figure 1**). All nanoparticles were thoroughly characterized for their composition, purity, size, surface area, shape, crystallinity, rate of dissolution, and their ability to generate reactive oxygen species (ROS) in a cell free system. To perform *in vitro* screening, we established a protein-based dispersion protocol to better disperse nanoparticles in cell culture media and prevent particle aggregation that could interfere with the interpretation of toxicological screening.[11,12] With respect to the initial three metal oxides, we found that nanoscale ZnO was very toxic to multiple mammalian cell lines, while TiO_2 and CeO_2 were non-toxic under dark conditions.[13] Based on thorough physicochemical characterization of the nanoparticles, we identified the importance of particle dissolution and shedding of toxic Zn-ions in the mechanism by which ZnO induces toxicity in mammalian cells. We were also able to demonstrate that TiO_2 can be rendered toxic by photoactivation, but this required tuning of the material bandgap in order to allow the use of non-toxic UV wavelengths for cellular screening.
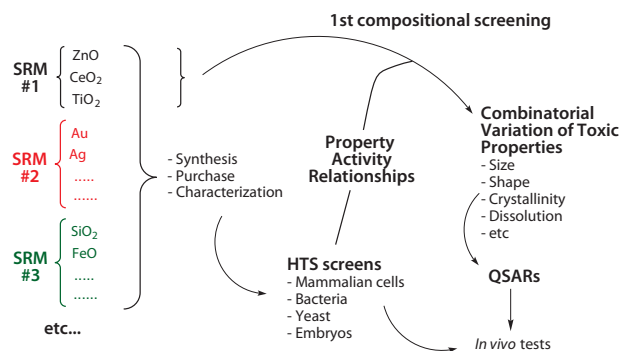
Figure 1. Building of compositional and combinatorial ENM libraries. This process involves selection of well-characterized standard reference materials with similar size and surface area, and obtained either by in-house synthesis or from commercial sources. The libraries can be grouped into metals, metal oxides, carbon or silica-based nanomaterials. The materials in each library are subjected to high throughput screening in various screening systems such as mammalian cells, bacteria, yeast, and zebrafish. The identified toxic materials are used to develop combinatorial libraries that contain variations of the potential toxic properties of the ENM. The information obtained from the ENM screening can be subsequently used to build quantitative structure-activity relationship (QSAR) models. Selected ENMs will be used in *in vivo* assays to validate the results obtained from *in vitro* screening.

To establish the link from specific physicochemical properties of an ENM to its toxicity, it is necessary to establish combinatorial libraries, synthesized to vary or alter major physicochemical properties that may be involved in toxicity. Property variations may include nanoparticle size, surface area, shape, crystallinity, bandgap, porosity, solubility, charge, and surface functionalization (**Figure 2**). Since we identified the importance of dissolution in ZnO-induced toxicity, we hypothesized that modifications of this material could alter the dissolution rate and modify its toxicity.
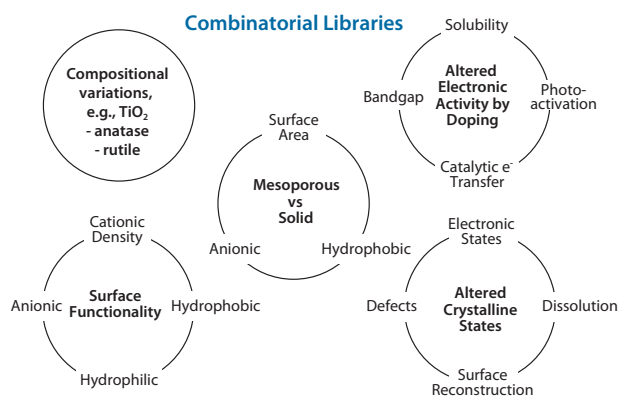
Figure 2. Examples of combinatorial ENM libraries. Combinatorial libraries are built by synthesizing one of the compositional materials to vary one of their major physicochemical properties that may be involved in toxicity. Property variations may include nanoparticle size, shape, porosity, hydrophilicity/hydrophobicity, crystallinity, bandgap, photoactivation, solubility, charge, and surface area. A single property variation may also change other properties, and rigorous re-characterization is required.

One way to achieve this is to introduce another element, iron, into ZnO during the nanoparticle synthesis. Through careful synthesis we obtained an Fe-doped ZnO combinatorial library that included a series of nanoparticles with incremental percentages of Fe. Characterization of this nanoparticle library showed that increasing percentages of Fe-doping decreased the ZnO dissolution rate in aqueous solutions without changing the crystal structure of the ZnO.[14] We then tested the toxicity of these nanoparticles *in vitro* and found that the cytotoxicity decreased as the percentage of Fe doping increased, indicating that dissolution rate indeed plays an important role in cytotoxicity. Currently, we are performing *in vivo* tests using the Fe-doped ZnO library and preliminary data shows that the *in vitro* findings extend to multiple animal models including zebrafish, mouse and rat. These results show that building compositional ENM libraries can quickly identify potentially toxic nanomaterials and that modifying nanomaterial properties to build combinatorial ENM libraries can help link specific physicochemical properties to toxicological outcomes.

Development of *In Vitro* Screening Assays

Much of the knowledge about ENM cellular toxicity has been generated using fairly straightforward cellular viability assays such as the lactate dehydrogenase (LDH) and the colorimetric MTT/MTS assays or propidium iodide (PI) staining. The major drawback is that these assays are often not informative of a specific toxicological pathway because multiple stimuli can result in the same assay outcome, establishing little connectivity between the biological outcome and specific ENM properties. Moreover, cellular viability assays also do not reflect sub-lethal toxicity effects. For these reasons we advocate developing mechanism-based *in vitro* assays because this is conceptually the easiest way to link *in vitro* toxicity screening with pathological effects *in vivo*. Currently, there are approximately ten major mechanistic pathways of toxicity that have been linked to ENMs (**Table 1**). These include injury paradigms such as the generation of reactive oxygen species and

oxidative stress, frustrated phagocytosis (e.g., in mesothelial surfaces), changes in protein structure and function (e.g., loss of enzymatic activity), protein unfolding response, immune response activation (e.g., through exposure of cryptic epitopes or immunostimulatory effects), fibrogenesis and tissue remodeling, blood clotting, vascular injury, neurotoxicity (e.g., oxidative stress, protein fibrillation), and genotoxicity.

Table 1. Experimental examples of major toxicological pathways that could lead to nanomaterial (ENM) toxicity (NPs = Nanoparticles, UFPs = UltraFine Particles)

Toxicological Pathway	Example Nanomaterials
Membrane damage/leakage/thinning	Cationic NPs
Protein binding/unfolding responses/loss of function/fibrillation	Metal oxide NPs, polystyrene, dendrimer, carbon nanomaterials
DNA cleavage/mutation	Nano-Ag
Mitochondrial damage: e-transfer/ATP/ PTP opening/apoptosis	UFPs, Cationic NPs
Lysosomal damage: proton pump activity/lysis/ frustrated phagocytosis	UFPs, Cationic NPs, CNTs
Inflammation: signaling cascades/cytokines/ chemokines/adhesion	Metal oxide NPs, CNTs
Fibrogenesis and tissue remodeling injury	CNTs
Blood platelet, vascular endothelial and clotting abnormalities	SiO$_2$
Oxidative stress injury, radical production, GSH depletion, lipid peroxidation, membrane oxidation, protein oxidation	UFPs, CNTs, Metal oxide NPs, Cationic NPs

It is important to note that additional mechanisms of toxicity are possible given the wide range of novel ENM physicochemical properties. For the purposes of this article, we will focus on the generation of oxidative stress.

Rapid Throughput Screening for *In Vitro* Pathway Assessment

Particle-induced oxidative stress invokes three tiers of cellular responses including cellular antioxidant defense, activation of pro-inflammatory signaling pathways leading to the production of cytokines/chemokines, and mitochondria-mediated cell death.[3,9,14,15] However, performing the entire panel of tests necessary to study the three tiers of oxidative stress requires at least 2-3 weeks of labor-intensive effort. A rapid throughput screening approach could offer several advantages over conventional assays. First, this approach speeds up the pace of knowledge generation that is possible with compositional and combinatorial ENM libraries. High throughput screening (HTS) provides a rapid readout because of the standardization of the procedure, automation (e.g., cell seeding, liquid handling, imaging, image analysis), and miniaturization (requiring smaller amounts of reagents and lowering the cost per assay). Not only is HTS capable of screening large libraries, but it can also accommodate multiple cell lines, time points and doses of exposure within the same experiment. Coupled with good bioinformatics and decision making tools, this approach can significantly improve the reliability of toxicological screening as well as establishment of property-activity relationships. To develop rapid throughput platforms based on mechanisms of toxicity, it is advantageous to combine different steps or nodal points in the injury pathway. Such multi-parametric screening efforts enhance the utility of the procedure, cover lethal and sublethal cellular responses and improve the predictive value of the assay. As an example of such an assay, we recently developed a multi-parametric screening procedure that incorporates several of the cellular oxidative stress responses involved in the advanced tier of oxidative stress (**Figure 3**).[14]

For questions, product data, or new product suggestions, please contact Aldrich Materials Science at *matsci@sial.com*.

83
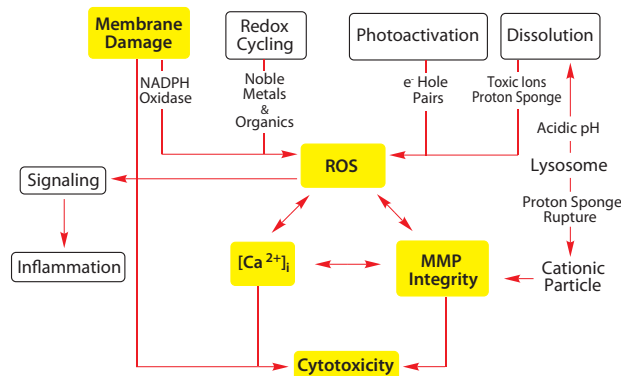
Figure 3. Schematic illustrating the relationships of cellular responses induced by metal oxide nanomaterials. We established multi-parametric HTS assays based on nanoparticle-induced Reactive Oxygen Species (ROS) production and oxidative stress. Nanomaterials induce ROS production as a direct consequence of specific material properties or as a consequence of triggering cellular injury responses leading to generation of the oxidant radicals. ROS production could trigger a range of oxidative stress effects. The induction of cellular toxicity at the highest level of oxidative stress involves a number of interrelated cellular responses, including intracellular Ca^{2+} release and perturbation of the mitochondrial membrane potential (MMP) that prestages cell death and the accompanying changes in cell membrane integrity and nuclear propidium iodide (PI) uptake. The parameters chosen in multi-parametric HTS assays are highlighted in yellow.

Prioritization of *In Vivo* Assays and Development of Quantitative Structure Activity Relationship (QSAR) Models

In vivo screening is time consuming and expensive. A complete set of toxicological assays for a single chemical, including assessment of carcinogenicity, chronic, reproduction and developmental effects could involve hundreds of animals and costs in the range of $1–3 million per test. As a result, less than 2% of industrial chemicals have undergone toxicity testing in rodents. We believe that by using a predictive toxicology approach it is possible to avoid a similar conundrum in nano-safety testing. Using the mechanism-based *in vitro* HTS screening, we should be able to identify the major mechanisms of toxicity and perform hazard ranking, which can then be used to prioritize *in vivo* testing. This approach also allows us to obtain data on the dose and kinetics related to the nanomaterial physicochemical properties, and to quantify biological response and exposure outcomes. The *in vivo* results are important to validate the *in vitro* screening as "predictive," thereby allowing the *in vitro* platform to be used as the primary screening procedure. *In vitro* HTS data will also be used to establish *in vitro* nano-QSARs by *in silico* modeling that will use statistics, mathematics and machine learning to perform hazard ranking as a prelude to future risk prediction studies.

Conclusion

We propose the implementation of predictive toxicology for toxicity screening of nanomaterials. This exercise is based on the establishment of compositional and combinatorial libraries, the development of mechanism-based *in vitro* toxicity screening assays, the development of multi-parametric high throughput screening assays, the building of computerized QSAR models, and the prioritization of *in vivo* assays to validate the predictability of *in vitro* assays. We think this is an appropriate approach to building a knowledge base that can meet the challenges of an expanding nanotechnology enterprise.

Acknowledgments

References
(1) Nel, A.; Xia, T.; Madler, L.; Li, N. *Science* **2006**, *311*, 622-627.
(2) Oberdorster, G.; Maynard, A.; Donaldson, K.; Castranova, V.; Fitzpatrick, J.; Ausman, K.; Carter, J.; Karn, B.; Kreyling, W.; Lai, D.; Olin, S.; Monteiro-Riviere, N.; Warheit, D.; Yang, H. *Part. Fibre. Toxicol.* **2005**, *2*, 8.
(3) Xia, T.; Li, N.; Nel, A. E. *Annu. Rev. Public Health* **2009**.
(4) Meng, H.; Xia, T.; George, S.; Nel, A. E. *ACS Nano* **2009**, *3*, 1620-1627.
(5) National Research Council. Toxicity Testing in the 21st Century: A Vision and a Strategy. http://dels.nas.edu/dels/rptbriefs/ToxicityTestingfinal.pdf. (Accessed 2007).
(6) National Toxicology Program. Toxicology in the 21st Century: The Role of the National Toxicology Program. http://ntp.niehs.nih.gov/ntp/main_pages/NTPVision.pdf (Accessed 2004).
(7) Walker, N. J.; Bucher, J. R. *Toxicol. Sci.* **2009**, *110*, 251-254.
(8) Nel, A. E.; Madler, L.; Velegol, D.; Xia, T.; Hoek, E. M.; Somasundaran, P.; Klaessig, F.; Castranova, V.; Thompson, M. *Nat. Mater.* **2009**, *8*, 543-557.
(9) Xia, T.; Kovochich, M.; Brant, J.; Hotze, M.; Sempf, J.; Oberley, T.; Sioutas, C.; Yeh, J. I.; Wiesner, M. R.; Nel, A. E. *Nano Lett.* **2006**, *6*, 1794-1807.
(10) Xia, T.; Kovochich, M.; Liong, M.; Zink, J. I.; Nel, A. E. *ACS Nano* **2008**, *2*, 85-96.
(11) Ji, Z.; Jin, X.; George, S.; Xia, T.; Meng, H.; Wang, X.; Suarez, E.; Zhang, H.; Hoek, E. M.; Godwin, H.; Nel, A. E.; Zink, J. I. *Environ. Sci. Technol.* **2010**, Article ASAP DOI: 10.1021/es100417s.
(12) Xia, T.; Kovochich, M.; Liong, M.; Meng, H.; Kabehie, S.; George, S.; Zink, J. I.; Nel, A. E. *ACS Nano* **2009**, *3*, 3273-86.
(13) Xia, T.; Kovochich, M.; Liong, M.; Madler, L.; Gilbert, B.; Shi, H.; Yeh, J. I.; Zink, J. I.; Nel, A. E. *ACS Nano* **2008**, *2*, 2121-2134.
(14) George, S.; Pokhrel, S.; Xia, T.; Gilbert, B.; Ji, Z.; Schowalter, M.; Rosenauer, A.; Damoiseaux, R.; Bradley, K. A.; Madler, L.; Nel, A. E. *ACS Nano* **2010**, *4*, 15-29.
(15) Li, N.; Xia, T.; Nel, A. E. *Free Radic. Biol. Med.* **2008**, *44*, 1689-1699.

Nanoparticles for Biomedical Applications

For a complete list of available nanomaterials, please visit *aldrich.com/nano*

Magnetic Nanoparticles

Name	Structure	Particle Dimensions	Concentration	Cat. No.
Iron oxide, magnetic nanoparticles solution	Fe_3O_4	avg. part. size 5 nm particle size 4 - 6 nm	5 mg/mL in H_2O	725331-5ML
Iron oxide, magnetic nanoparticles solution	Fe_3O_4	avg. part. size 10 nm particle size 9 - 11 nm	10 mg/mL in H_2O	725358-5ML
Iron oxide, magnetic nanoparticles solution	Fe_3O_4	avg. part. size 20 nm particle size 18 - 22 nm	5 mg/mL in H_2O	725366-5ML
Iron oxide, magnetic nanoparticles solution solution	Fe_3O_4	avg. part. size 5 nm particle size 4.5 - 5.5 nm (TEM)	5 mg/mL in toluene	700320-5ML
Iron oxide, magnetic nanoparticles solution solution	Fe_3O_4	avg. part. size 10 nm particle size 9 - 11 nm (TEM)	5 mg/mL in toluene	700312-5ML
Iron oxide, magnetic nanoparticles solution solution	Fe_3O_4	avg. part. size 20 nm particle size 18 - 22 nm (TEM)	5 mg/mL in toluene	700304-5ML
Cobalt Carbon coated (magnetic) Carbon content < 8 wt. % nanopowder	Co	particle size <50 nm (TEM)	≥99%	697745-500MG

Quantum Dots

Name	Composition	Spectroscopic Properties	Cat. No.
Lumidot™ CdS, 380, 5 mg/mL in toluene	CdS	λ_{abs} 350-370 nm, λ_{em} = 370-390 nm	662429-10ML
Lumidot™ CdS, 400, 5 mg/mL in toluene	CdS	λ_{abs} 370-390 nm, λ_{em} = 390-410 nm	662410-10ML
Lumidot™ CdS, 420, 5 mg/mL in toluene	CdS	λ_{abs} 390-410 nm, λ_{em} = 410-430 nm	662402-10ML
Lumidot™ CdS, 440, 5 mg/mL in toluene	CdS	λ_{abs} 410-430 nm, λ_{em} = 430-450 nm	662380-10ML
Lumidot™ CdS, 460, 5 mg/mL in toluene	CdS	λ_{abs} 430-450 nm, λ_{em} = 450-470 nm	662372-10ML
Lumidot™ CdS, 480, 5 mg/mL in toluene	CdS	λ_{abs} 450-470 nm, λ_{em} = 470-490 nm	662364-10ML
Lumidot™ CdS-6, quantum dot nanoparticles kit, core-shell type, 5 mg/mL in toluene	CdS	λ_{em} = 380-480 nm	662593-1KT
Lumidot™ CdSe, 480, 5 mg/mL in toluene	CdSe	λ_{abs} 455-465 nm, λ_{em} = 475-485 nm	662356-10ML
Lumidot™ CdSe, 520, 5 mg/mL in toluene	CdSe	λ_{abs} 495-505 nm, λ_{em} = 515-525 nm	662437-10ML
Lumidot™ CdSe, 560, 5 mg/mL in toluene	CdSe	λ_{abs} 535-545 nm, λ_{em} = 555-565 nm	662445-10ML
Lumidot™ CdSe, 590, 5 mg/mL in toluene	CdSe	λ_{abs} 565-575 nm, λ_{em} = 585-595 nm	662607-10ML
Lumidot™ CdSe, 610, 5 mg/mL in toluene	CdSe	λ_{abs} 585-595 nm, λ_{em} = 605-615 nm	662488-10ML
Lumidot™ CdSe, 640, 5 mg/mL in toluene	CdSe	λ_{abs} 615-625 nm, λ_{em} = 635-645 nm	662461-10ML
Lumidot™ CdSe-6, quantum dot nanoparticles kit, core-shell type, 5 mg/mL in toluene	CdS	λ_{em} = 480-640 nm	662550-1KT
Lumidot™ CdSe/ZnS, 480, 5 mg/mL in toluene*	CdSe/ZnS	λ_{em} = 480 nm	694592-2ML 694592-10ML
Lumidot™ CdSe/ZnS, 510, 5 mg/mL in toluene*	CdSe/ZnS	λ_{em} = 510 nm	694657-2ML 694657-10ML
Lumidot™ CdSe/ZnS, 530, 5 mg/mL in toluene*	CdSe/ZnS	λ_{em} = 530 nm	694649-2ML 694649-10ML
Lumidot™ CdSe/ZnS, 560, 5 mg/mL in toluene*	CdSe/ZnS	λ_{em} = 560 nm	694630-2ML 694630-10ML
Lumidot™ CdSe/ZnS, 590, 5 mg/mL in toluene*	CdSe/ZnS	λ_{em} = 590 nm	694622-2ML 694622-10ML
Lumidot™ CdSe/ZnS, 610, 5 mg/mL in toluene*	CdSe/ZnS	λ_{em} = 610 nm	694614-2ML 694614-10ML
Lumidot™ CdSe/ZnS, 640, 5 mg/mL in toluene*	CdSe/ZnS	λ_{em} = 640 nm	694606-2ML 694606-10ML

*Products not available in the United States

For questions, product data, or new product suggestions, please contact Aldrich Materials Science at *matsci@sial.com*.

85

Metal Oxides and Ceramics

For a complete list of available metal oxides and ceramics, please visit *aldrich.com/periodic*

Name	Composition	Particle Size	Purity/Concentration	Cat. No.
Hydroxyapatite nanopowder	$Ca_5(OH)(PO_4)_3$	<200 nm (BET)	≥97%	677418-5G 677418-10G 677418-25G
Hydroxyapatite nanopowder, silica 5 wt. % as dopant	$Ca_5(OH)(PO_4)_3$	<200 nm (BET)	-	693863-5G
Hydroxyapatite dispersion nanoparticles, ≤0.025 wt. % as dispersant (non-metal based)	$Ca_5(OH)(PO_4)_3$	<200 nm (BET)	10 wt. % in H_2O	702153-25ML
Tricalcium phosphate hydrate nanopowder	$Ca_3(PO_4)_2$	<200 nm (BET) <100 nm (TEM)	-	693898-5G
Aluminum oxide nanopowder	Al_2O_3	<50 nm (TEM)	-	544833-10G 544833-50G
Aluminum oxide nanopowder	Al_2O_3	13 nm	99.8% trace metals basis	718475-100G
Aluminum oxide, dispersion nanoparticles	Al_2O_3	<50 nm (TEM)	10 wt. % in H_2O	642991-100ML
Titanium(IV) oxide nanopowder	TiO_2	~21 nm	≥99.5% trace metals basis	718467-100G
Titanium(IV) oxide, mixture of rutile and anatase nanopowder	TiO_2	<100 nm (BET) <50 nm (XRD)	99.5% trace metals basis	634662-25G 634662-100G
Titanium(IV) oxide, mixture of rutile and anatase dispersion nanoparticles	TiO_2	~21 nm (primary particle size of starting nanopowder) <150 nm (DLS)	99.9% trace metals basis/ 33-37 wt. % in H_2O	700347-25G 700347-100G
Zirconium(IV) oxide nanopowder	ZrO_2	<100 nm (TEM)	-	544760-5G 544760-25G
Zirconium(IV) oxide, dispersion nanoparticles	ZrO_2	<100 nm (BET)	10 wt. % in H_2O	643025-100ML 643025-500ML

Mesoporous Materials

For a complete list of available mesoporous materials, please visit *aldrich.com/nano*

Name	Composition	Property	Cat. No.
Carbon, mesoporous	C	particle size distribution 45 μm ±5, average pore diameter 100 Å ±10 Å (typical) pore volume 0.5 cm³/g (typical), spec. surface area 150-250 m²/g	699640-5G 699640-25G
Carbon, mesoporous nanopowder	C	particle size <500 nm (DLS), average pore diameter 64 Å (typical) total pore volume 0.342 cm³/g (typical), spec. surface area 150-250 m²/g	699632-5G 699632-25G
Carbon, mesoporous hydrophilic pore surface	C	mesoporosity >0.4 cm³/g, spec. surface area >300 m²/g (BET) mesopore surface area ≥130 m²/g	702110-5G
Carbon, mesoporous hydrophobic pore surface	C	mesoporosity 0.4-0.7 cm³/g microporosity 0-0.2 cm³/g, spec. surface area 150-500 m²/g (BET)	702102-5G
Silica, mesostructured MCM-41 (hexagonal)	SiO_2	pore size 2.3-2.7 nm pore volume 0.98 cm³/g, spec. surface area ~1000 m²/g (BET)	643645-5G 643645-25G
Silica, mesostructured MSU-H (large pore 2D hexagonal)	SiO_2	pore size ~ 7.1 nm pore volume 0.91 cm³/g, spec. surface area ~750 m²/g (BET)	643637-5G 643637-25G
Silica, mesostructured MSU-F (cellular foam)	SiO_2	pore volume 2.31 cm³/g, spec. surface area 562 m²/g	560979-10G
Silica, mesostructured HMS (wormhole)	SiO_2	particle size 3.05 μm (avg.), pore size 3.9 nm (avg.) pore volume 1.76 cm³/g, spec. surface area 910 m²/g	541036-5G 541036-25G

Gold Nanomaterials

For a complete list of available gold nanomaterials, please visit *aldrich.com/periodic* and click on gold

Name	Composition	Dimension	Concentration	Cat. No.
Gold nanopowder	Au	particle size <100 nm	-	636347-1G
Octanethiol functionalized gold nanoparticles	-	particle size 2 - 4 nm (DLS)	2 % (w/v) in toluene	660426-5ML
Dodecanethiol functionalized gold nanoparticles	-	particle size 3 - 5 nm (TEM)	2 % (w/v) in toluene	660434-5ML
1-Mercapto-(triethylene glycol) methyl ether functionalized gold nanoparticles	-	particle size 3.5 - 5.5 nm (TEM)	2 % (w/v) in absolute ethanol	694169-5ML
(11-Mercaptoundecyl)tetra(ethylene glycol) functionalized gold nanoparticles	-	particle size 3.5 - 5.5 nm (TEM)	2 % (w/v) in H_2O	687863-5ML
Gold nanorods amine terminated λ_{abs}absorption 808 nm	Au	diameter 10 nm	1.8 mg/mL in H_2O	716871-1ML
Gold nanorods carboxyl terminated λ_{abs}absorption 808 nm	Au	diameter 10 nm	1.8 mg/mL in H_2O	716898-1ML
Gold nanorods methyl terminated λ_{abs}absorption 808 nm	Au	diameter 10 nm	1.8 mg/mL in H_2O	716901-1ML
Gold microrods	Au	diameter 200 nm	50 µg/mL in H_2O	716960-10ML

Silver Nanomaterials

For a complete list of available silver nanomaterials, please visit *aldrich.com/periodic* and click on silver

Name	Composition	Particle Size	Concentration	Cat. No.
Silver, nanoparticle dispersion	Ag	10 nm (TEM)	0.02 mg/mL in aqueous buffer	730785-25ML
Silver, nanoparticle dispersion	Ag	20 nm (TEM)	0.02 mg/mL in aqueous buffer	730793-25ML
Silver, nanoparticle dispersion	Ag	40 µm (TEM)	0.02 mg/mL in aqueous buffer	730807-25ML
Silver, nanoparticle dispersion	Ag	60 nm (TEM)	0.02 mg/mL in aqueous buffer	730815-25ML
Silver, nanoparticle dispersion	Ag	100 nm (TEM)	0.02 mg/mL in aqueous buffer	730777-25ML
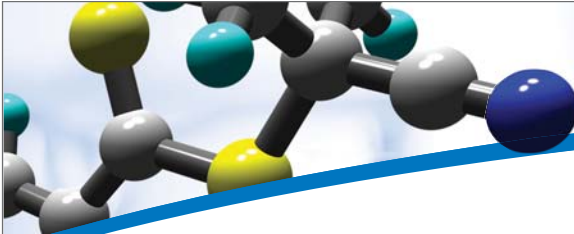
For questions, product data, or new product suggestions, please contact Aldrich Materials Science at *matsci@sial.com*.

87

Sigma-Aldrich
3050 Spruce Street
St. Louis, MO 63103 USA

Sigma-Aldrich® Worldwide Offices

Argentina
Free Tel: 0810 888 7446
Tel: (+54) 11 4556 1472
Fax: (+54) 11 4552 1698

Australia
Free Tel: 1800 800 097
Free Fax: 1800 800 096
Tel: (+61) 2 9841 0555
Fax: (+61) 2 9841 0500

Austria
Tel: (+43) 1 605 81 10
Fax: (+43) 1 605 81 20

Belgium
Free Tel: 0800 14747
Free Fax: 0800 14745
Tel: (+32) 3 899 13 01
Fax: (+32) 3 899 13 11

Brazil
Free Tel: 0800 701 7425
Tel: (+55) 11 3732 3100
Fax: (+55) 11 5522 9895

Canada
Free Tel: 1800 565 1400
Free Fax: 1800 265 3858
Tel: (+1) 905 829 9500
Fax: (+1) 905 829 9292

Chile
Tel: (+56) 2 495 7395
Fax: (+56) 2 495 7396

China
Free Tel: 800 819 3336
Tel: (+86) 21 6141 5566
Fax: (+86) 21 6141 5567

Czech Republic
Tel: (+420) 246 003 200
Fax: (+420) 246 003 291

Denmark
Tel: (+45) 43 56 59 00
Fax: (+45) 43 56 59 05

Finland
Tel: (+358) 9 350 9250
Fax: (+358) 9 350 92555

France
Free Tel: 0800 211 408
Free Fax: 0800 031 052
Tel: (+33) 474 82 28 88
Fax: (+33) 474 95 68 08

Germany
Free Tel: 0800 51 55 000
Free Fax: 0800 64 90 000
Tel: (+49) 89 6513 0
Fax: (+49) 89 6513 1160

Hungary
Ingyenes telefonszám: 06 80 355 355
Ingyenes fax szám: 06 80 344 344
Tel: (+36) 1 235 9063
Fax: (+36) 1 269 6470

India
Telephone
Bangalore: (+91) 80 6621 9400
New Delhi: (+91) 11 4358 8000
Mumbai: (+91) 22 4087 2364
Hyderabad: (+91) 40 4015 5488
Kolkata: (+91) 33 4013 8000

Fax
Bangalore: (+91) 80 6621 9550
New Delhi: (+91) 11 4358 8001
Mumbai: (+91) 22 2579 7589
Hyderabad: (+91) 40 4015 5466
Kolkata: (+91) 33 4013 8016

Ireland
Free Tel: 1800 200 888
Free Fax: 1800 600 222
Tel: (+353) 402 20370
Fax: (+ 353) 402 20375

Israel
Free Tel: 1 800 70 2222
Tel: (+972) 8 948 4100
Fax: (+972) 8 948 4200

Italy
Free Tel: 800 827 018
Tel: (+39) 02 3341 7310
Fax: (+39) 02 3801 0737

Japan
Tel: (+81) 3 5796 7300
Fax: (+81) 3 5796 7315

Korea
Free Tel: (+82) 80 023 7111
Free Fax: (+82) 80 023 8111
Tel: (+82) 31 329 9000
Fax: (+82) 31 329 9090

Malaysia
Tel: (+60) 3 5635 3321
Fax: (+60) 3 5635 4116

Mexico
Free Tel: 01 800 007 5300
Free Fax: 01 800 712 9920
Tel: (+52) 722 276 1600
Fax: (+52) 722 276 1601

The Netherlands
Free Tel: 0800 022 9088
Free Fax: 0800 022 9089
Tel: (+31) 78 620 5411
Fax: (+31) 78 620 5421

New Zealand
Free Tel: 0800 936 666
Free Fax: 0800 937 777
Tel: (+61) 2 9841 0555
Fax: (+61) 2 9841 0500

Norway
Tel: (+47) 23 17 60 00
Fax: (+47) 23 17 60 10

Poland
Tel: (+48) 61 829 01 00
Fax: (+48) 61 829 01 20

Portugal
Free Tel: 800 202 180
Free Fax: 800 202 178
Tel: (+351) 21 924 2555
Fax: (+351) 21 924 2610

Russia
Tel: (+7) 495 621 5828
Fax: (+7) 495 621 6037

Singapore
Tel: (+65) 6779 1200
Fax: (+65) 6779 1822

Slovakia
Tel: (+421) 255 571 562
Fax: (+421) 255 571 564

South Africa
Free Tel: 0800 1100 75
Free Fax: 0800 1100 79
Tel: (+27) 11 979 1188
Fax: (+27) 11 979 1119

Spain
Free Tel: 900 101 376
Free Fax: 900 102 028
Tel: (+34) 91 661 99 77
Fax: (+34) 91 661 96 42

Sweden
Tel: (+46) 8 742 4200
Fax: (+46) 8 742 4243

Switzerland
Free Tel: 0800 80 00 80
Free Fax: 0800 80 00 81
Tel: (+41) 81 755 2828
Fax: (+41) 81 755 2815

United Kingdom
Free Tel: 0800 717 181
Free Fax: 0800 378 785
Tel: (+44) 1747 833 000
Fax: (+44) 1747 833 313

United States
Toll-Free: 800 325 3010
Toll-Free Fax: 800 325 5052
Tel: (+1) 314 771 5765
Fax: (+1) 314 771 5757

Vietnam
Tel: (+84) 3516 2810
Fax: (+84) 6258 4238

Internet
sigma-aldrich.com

Green U Power

© **Mixed Sources**
Product group from well-managed
forests, controlled sources and
recycled wood or fiber
www.fsc.org Cert no. SGS-COC-003338
© 1996 Forest Stewardship Council
FSC   10%

Enabling Science to
Improve the Quality of Life

Order/Customer Service (800) 325-3010 • Fax (800) 325-5052
Technical Service (800) 325-5832 • *sigma-aldrich.com/techservice*
Development/Custom Manufacturing Inquiries SAFC® (800) 244-1173
Safety-related Information *sigma-aldrich.com/safetycenter*

World Headquarters
3050 Spruce St.
St. Louis, MO 63103
(314) 771-5765
sigma-aldrich.com

MSI
74201-510901
1090

SIGMA-ALDRICH®